

1 **Improved representation of plant physiology in the JULES-**
2 **vn5.6 land surface model: Photosynthesis, stomatal**
3 **conductance and thermal acclimation**

4
5 Rebecca J. Oliver¹, Lina M. Mercado^{1,2}, Doug B. Clark¹, Chris Huntingford¹, Christopher M. Taylor^{1,5}, Pier Luigi
6 Vidale³, Patrick C. McGuire³, Markus Todt³, Sonja Folwell¹, Valiyaveetil Shamsudheen Semeena¹, Belinda E.
7 Medlyn⁴

8
9 ¹ UK Centre for Ecology and Hydrology, Wallingford, OX10 8BB, UK

10 ² College of Life and Environmental Sciences, University of Exeter, Exeter, EX4 4RJ, UK

11 ³ Department of Meteorology and National Centre for Atmospheric Science, Reading University, Reading RG6
12 6BB, UK

13 ⁴ Hawkesbury Institute for the Environment, Western Sydney University, Australia

14 ⁵ National Centre for Earth Observation, Wallingford, OX10 8BB, UK

15 Journal: GMD – Development and technical paper

16 *Correspondence to:* R. J. Oliver (rfu@ceh.ac.uk)

29 **Abstract.**

30 Carbon and water cycle dynamics of vegetation are controlled primarily by photosynthesis and stomatal
31 conductance (g_s). Our goal is to improve the representation of these key physiological processes within the JULES
32 land surface model, with a particular focus on refining the temperature sensitivity of photosynthesis, impacting
33 modelled carbon, energy and water fluxes. We test (1) an implementation of the Farquhar et al. (1980)
34 photosynthesis scheme and associated plant functional type-dependent photosynthetic temperature response
35 functions, (2) the optimality-based g_s scheme from Medlyn et al. (2011), and (3) the Kattge and Knorr (2007)
36 photosynthetic capacity thermal acclimation scheme. New parameters for each model configuration are adopted
37 from recent large observational datasets that synthesise global experimental data. These developments to JULES
38 incorporate current physiological understanding of vegetation behaviour into the model, and enable users to derive
39 direct links between model parameters and on-going measurement campaigns that refine such parameter values.
40 Replacement of the original Collatz *et al.* (1991) C_3 photosynthesis model with the Farquhar scheme results in
41 large changes in GPP for current-day, with ~10% reduction in seasonal (June-August; JJA and December-
42 February; DJF) mean GPP in tropical forests, and ~20% increase in the northern high latitude forests in JJA. The
43 optimality-based g_s model decreases the latent heat flux for the present-day (~10%, with an associated increase in
44 sensible heat flux) across regions dominated by needleleaf evergreen forest in the northern hemisphere summer.
45 Thermal acclimation of photosynthesis coupled with the Medlyn g_s scheme reduced tropical forest GPP by up to
46 5%, and increased GPP in the high northern latitude forests by between 2 to 5%. Evaluation of simulated carbon
47 and water fluxes by each model configuration against global data products show this latter configuration generates
48 improvements in these key areas. Thermal acclimation of photosynthesis coupled with the Medlyn g_s scheme
49 improved modelled carbon fluxes in tropical and high northern latitude forests in JJA, and improved the simulation
50 of evapotranspiration across much of the northern hemisphere in JJA. Having established good model
51 performance for the contemporary period, we force this new version of JULES offline with a future climate
52 scenario corresponding to rising atmospheric greenhouse gases (SSP5 RCP8.5). In particular, these calculations
53 allow understanding of the effects of long-term warming. We find that the impact of thermal acclimation coupled
54 with the optimality-based g_s model on simulated fluxes increases latent heat flux (+50%) by year 2050 compared
55 to the JULES model configuration without acclimation. This new JULES configuration also projects increased
56 GPP across tropical (+10%) and northern latitude regions (+30%) by 2050. We conclude that thermal acclimation
57 of photosynthesis with the Farquhar photosynthesis scheme and the new optimality-based g_s scheme together
58 improve the simulation of carbon and water fluxes for current-day, and has a large impact on modelled future
59 carbon cycle dynamics in a warming world.

60

61

62

63

64

65 **1. Introduction**

66 Photosynthesis and stomatal conductance (g_s) together exert a strong control over the exchange of carbon, water
67 and energy between the land surface and the atmosphere. The behaviour of stomatal pores on the leaf surface link
68 these processes, controlling the amount of carbon dioxide (CO_2) entering, and water leaving each leaf.
69 Photosynthesis represents the largest exchange of carbon between the land and atmosphere (Friedlingstein et al.,
70 2020), being more substantial than respiration loss. This imbalance is central to the global carbon cycle because
71 it slows the rate of accumulation of CO_2 in the atmosphere caused by fossil fuel burning, and therefore also lowers
72 the rate of atmospheric temperature increase. As stomata open to take up CO_2 for photosynthesis, plants also lose
73 water through transpiration, and this flux has been estimated to account for 60–80% of evapotranspiration (ET)
74 across the land surface (Jasechko et al., 2013; Schlesinger and Jasechko, 2014). Hence, for vegetated surfaces,
75 transpiration is the primary driver of the latent heat flux (LE), the latter describing the overall transfer of water
76 vapour to the atmosphere. The partitioning of available net radiation between LE and sensible heat (H) is also a
77 key determinant of land surface temperature, therefore having a feedback on photosynthesis and other key
78 metabolic processes that influence the global carbon cycle such as plant respiration.

79 Land surface models (LSMs) simulate the exchange of carbon, water and energy between the land surface and the
80 atmosphere, providing the lower boundary conditions for the atmospheric component of Earth System Models
81 (ESMs) when run in a coupled configuration. ESM projections form the main tool to predict future climate change
82 and underpin much of the regular United Nations Intergovernmental Panel on Climate Change (IPCC) reports that
83 inform policymakers. However, ESM predictions of the global carbon sink are fraught with large uncertainties
84 surrounding projections of future carbon uptake (Friedlingstein et al., 2014), causing uncertainty in any translation
85 from CO_2 emissions to atmospheric CO_2 trajectory. A lack of knowledge in how the global carbon cycle operates
86 creates uncertainties in translating from emissions to global warming, and these uncertainties are a sizeable
87 fraction of those associated with unknowns of physical climate processes (Huntingford et al., 2009). Therefore,
88 given the critical role of both photosynthesis and g_s in determining land-atmosphere exchanges, their accurate
89 representation and parameterisation in LSMs is of paramount importance. Booth et al. (2012) show that a
90 significant uncertainty is the temperature sensitivity of photosynthesis, and suggest that thermal acclimation of
91 photosynthesis – where plants adjust their optimum temperature for photosynthesis to growth conditions
92 experienced over the timescale of days to weeks - might reduce the spread in modelled carbon exchange. Yet
93 despite strong evidence of the thermal acclimation capability of plant photosynthesis (Dusenge et al., 2020; Slot
94 et al., 2021; Way et al., 2017; Way and Yamori, 2014; Yamaguchi et al., 2016), incorporation of this process in
95 large-scale LSMs is limited to only a few e.g. TEM (Chen and Zhuang, 2013), CLM4.5 (Lombardozzi et al.,
96 2015), LM3 (Smith et al., 2016), JULES (Mercado et al., 2018), ORCHIDEE (Krinner et al., 2005) and BETHY
97 (Ziehn et al., 2011), and is not yet commonly represented in ESMs. Currently, the majority of LSMs and ESMs
98 use simple fixed (i.e. non-acclimating) temperature response functions for photosynthetic capacity parameters
99 (Smith and Dukes, 2013), which, in general, cause the rate of leaf photosynthesis to increase with temperature to
100 an optimum and then decrease under higher temperatures. These functional forms are either generic for all C_3/C_4
101 species and fixed in time and space, or are dependent on a small number of plant functional types (PFTs) but again
102 fixed in time and space. Consequently, climate-carbon feedbacks in ESMs are sensitive to the assumed value of
103 the fixed optimum temperature for photosynthetic capacity (T_{opt}), because, ~~very simplistically,~~ the amount of

104 carbon assimilated depends on whether leaf temperature is dominantly above or below T_{opt} . Improved process
105 representation of g_s , photosynthesis, and its temperature sensitivity in LSMs is necessary to support robust
106 predictions of global climate change via their coupling into ESMS. Modelling studies have shown how
107 photosynthesis and g_s impact climate feedbacks, play a critical role in how climate will change, and strongly
108 influence climate-induced impacts such as water resources (Betts et al., 2007; Cruz et al., 2010; De Arellano et
109 al., 2012; Gedney et al., 2006; Kooperman et al., 2018; Zeng et al., 2017).

110 This study, therefore, updates the plant physiology routines in the Joint UK Land Surface Environment Simulator
111 (JULES-vn5.6) LSM, the land-surface component of the UK Hadley Centre ESM (Sellar et al., 2019). To date,
112 JULES has employed the mechanistic C_3 photosynthesis scheme of Collatz et al. (1991) (“Collatz”). However,
113 the Farquhar et al. (1980) (“Farquhar”) scheme is more generally adopted by those modelling photosynthetic
114 response and by researchers analysing data from empirical studies. The Farquhar scheme has been recently
115 implemented in JULES by Mercado et al. (2018) for C_3 plant types, albeit using a big leaf canopy scaling approach
116 and was not parameterised and evaluated for global applications. Here we build on that previous study by using a
117 data-driven approach incorporating data from multiple biomes to parameterise the Farquhar model photosynthetic
118 capacity parameters and their temperature sensitivity so it is amenable for use in global studies. Our specific
119 rationale for including the Farquhar photosynthesis scheme is twofold. Firstly, studies by Rogers et al. (2017) and
120 Walker et al. (2021) demonstrate that despite only the Collatz or Farquhar descriptions of leaf photosynthesis
121 being in general use, simulated photosynthesis varies significantly between LSMs. This variation is attributed to
122 several factors, including 1) differences in prescribed Rubisco kinetic constants and their temperature responses
123 (Rogers et al., 2017), 2) structural differences, namely the method used to determine the transition point between
124 the limiting rates of photosynthesis which has a disproportionate impact on estimates (Huntingford and Oliver,
125 2021; Walker et al., 2021), and 3) the sensitivity of photosynthesis to temperature, in terms of the under-
126 representation of parameters from different biomes to describe the short-term instantaneous response of
127 photosynthesis to temperature (Rogers et al., 2017). In particular, these differences imply that parameter values
128 derived calibrating the Collatz model against data will differ to those derived using Farquhar against the same set
129 of measurements. Parameter values are not transferable between models, hence such differences will lead to
130 inconsistencies and projection errors if parameters are fitted to data, but then applied within the alternative model.
131 Building in the capacity of an LSM to run with either photosynthesis scheme greatly enhances flexibility in
132 modelling. Importantly, this flexibility allows for consistency between parameters used by empiricists to derive
133 leaf level photosynthetic parameters from observations, and those used in large scale modelling. Additionally, our
134 re-parameterisation of the photosynthetic capacity and temperature sensitivity parameters are based on recent
135 global datasets that are more extensive, including species from a range of different biomes, further enhancing the
136 capacity for global modelling applications. Our second rationale is that the Farquhar photosynthesis scheme is
137 required as the underlying model to implement the Kattge and Knorr (2007) thermal acclimation scheme.

138 Leaf level g_s response to water vapour is commonly represented in LSMs empirically (Jarvis et al., 1976), or with
139 a semi-empirical model (Ball et al., 1987; Damour et al., 2010; Leuning, 1995). Values of g_s are subsequently
140 scaled yielding an estimate of canopy conductance for vegetation in different ecosystems. De Kauwe et al. (2013)
141 showed that 10 of the 11 ecosystem models studied in their inter-comparison used a form of the “Ball–Berry–
142 Leuning” approximation. This model form links g_s to changes in environmental conditions, and directly to

143 photosynthetic rate. However, there is increasing interest in using models based on optimisation theory (Franks et
144 al., 2017; Franks et al., 2018), using evidence that stomata may behave to maximise CO₂ gain whilst minimising
145 water loss. The major advantage of optimality theory is that the optimisation criterion will apply under any
146 environmental conditions, past or future. Hence the derived equations can replace uncertain mechanistic
147 formulations and may also have more predictive capability corresponding to future climate regimes. JULES
148 traditionally uses the empirically-based Jacobs (1994) g_s scheme (“Jacobs”), and in this study we compare the
149 behaviour of this scheme against the Medlyn et al. (2011) g_s scheme (“Medlyn”) which is based on optimisation
150 theory. The Medlyn g_s model has been previously implemented in JULES by Oliver et al. (2018). However, in
151 this study, we advance on that previous work by calibrating for the increased number of plant functional types
152 now in JULES (nine PFTs, as opposed to five in the original study), and we parameterise using data from a global
153 synthesis of experimental observations.

154 There is increasing evidence that the short-term vegetation temperature responses are themselves sensitive to
155 temperatures experienced over longer time-scales (days to weeks to seasons) and in particular, have the capability
156 to acclimate to growth temperature (T_{growth}) (Kattge and Knorr, 2007). Observational evidence of thermal
157 acclimation of photosynthesis has been widely reported, primarily for temperate and boreal ecosystems (Atkin et
158 al., 2006; Gunderson et al., 2000; Gunderson et al., 2010; Hikosaka et al., 2007; Way and Yamori, 2014; Yamori
159 et al., 2014). The effect is defined as the fast temporal adjustment of the temperature response of photosynthesis
160 driven by a change in T_{growth} . Thermal acclimation of photosynthesis typically results in a shift in the optimum
161 temperature (T_{opt}) for photosynthesis towards the new growth temperature, which can result in an increase or
162 maintenance of the photosynthetic rate respective to T_{growth} (Yamori et al., 2014). In this study, we implement
163 thermal acclimation of photosynthetic capacity in JULES using the scheme from Kattge and Knorr (2007). The
164 scheme attributes all changes in the photosynthetic response to changing T_{growth} , without specifically separating
165 adaptation from acclimation processes. Of those LSMs that do account for thermal acclimation of photosynthesis
166 (e.g. TEM, CLM4.5, LM3, JULES) (Chen and Zhuang, 2013; Lombardozzi et al., 2015; Mercado et al., 2018;
167 Smith et al., 2016), all similarly use this numerical algorithm from Kattge and Knorr (2007). Mercado et al. (2018)
168 investigated the impacts of thermal acclimation on the future land carbon sink using an implementation of the
169 Kattge and Knorr (2007) in JULES, although using a simple big leaf scaling approach. In this study we apply the
170 thermal acclimation scheme in the updated JULES model (i.e. newly parameterised Farquhar scheme, running
171 with a multi-layer canopy and nine PFTs) and updated with the Medlyn g_s scheme and related parameters.

172 This paper therefore brings together these three key recent developments of the JULES plant physiology routines,
173 (1) implementation of the Farquhar photosynthesis scheme, (2) the optimisation-based Medlyn model of stomatal
174 opening, and (3) thermal acclimation of photosynthesis, along with updated parameters and an evaluation of model
175 behaviour. We make incremental additions of the different processes to the JULES model in a set of factorial
176 simulations and run the model with current day (1979 to 2013) near-surface meteorological forcing and CO₂
177 levels. First, we present the different factorial simulations in the context of a thorough evaluation of simulated
178 contemporary carbon and energy fluxes. Such evaluation includes comparison against individual eddy covariance
179 sites, and at spatial scales up to the global scale against satellite products. Timescales analysed are both seasonal
180 and annual. Secondly, we apply the new model configurations within a past-to-future climate change simulation
181 based on a high-end emissions scenario (SSP5 RCP8.5). We use output from HadGEM3-GC3.1 spanning years

Formatted: Font: Not Italic

182 1960 to 2050 to explore sensitivity of global vegetation to future climate change. This choice of scenario is to
183 allow eventual comparison between these offline simulations and the equivalent in the coupled global climate
184 model to investigate land-atmosphere feedbacks resulting from these changes to the plant physiology routines.
185 This is currently work being undertaken. This updated version of the JULES model is now available in official
186 JULES releases for use by the community (see data availability). It is therefore also readily available for full
187 coupling into the UK community ESM (UKESM), a process that is just starting.

188

189 **2. Model description**

190 **2.1 JULES land surface model**

191 Our modelling framework is JULES (<https://jules.jchmr.org>), the land surface component of the Hadley Centre
192 climate models, which includes the new UK community Earth System Model (UKESM1) (Sellar et al., 2019).
193 JULES can be run offline, as in this study, forced with observed meteorology, at different spatial scales (from a
194 single location to global). A full description of JULES is provided in Best et al. (2011), Clark et al. (2011) and
195 Harper et al. (2016). Of particular relevance for this study is the plant physiological representation in JULES.
196 JULES uses a leaf-level coupled model of photosynthesis and g_s (Cox et al., 1998) based on Collatz et al. (1991)
197 and Collatz et al. (1992) (for C_3 and C_4 plants) and Jacobs (1994) respectively. Photosynthesis and g_s are modelled
198 to respond to changes in environmental drivers of temperature, humidity deficit, light, CO_2 concentration and
199 water availability. Soil moisture content is modelled using a dimensionless soil water stress factor which is related
200 to the mean soil water concentration in the root zone, and the soil water contents at the critical and wilting point
201 (Best et al., 2011). [The critical and wilting point soil moisture concentrations vary by soil type in these simulations.](#)
202 In this study, JULES uses a multilayer canopy radiation interception and photosynthesis scheme (i.e. 10 layers)
203 that accounts for vertical variation of incoming direct and diffuse radiation, sun fleck penetration through the
204 canopy, change in photosynthetic capacity with depth into the canopy, inhibition of leaf respiration in the light
205 and differentiates calculation of sunlit and shaded photosynthesis at each layer (Clark et al., 2011; Mercado et al.,
206 2009). [The implementation of a multilayer canopy for light interception in JULES was shown to improve modelled
canopy scale photosynthetic fluxes at eddy covariance sites compared to the 'big leaf approach' \(Blyth et al.,
207 2011; Jogireddy et al., 2006; Mercado et al., 2007\). Specifically, the multi-layer approach better captured the light
208 response and diurnal cycles of canopy photosynthesis. While light inhibition of leaf respiration and changing
209 photosynthetic capacity with canopy depth are supported by observations \(Atkin et al., 2000; Atkin et al., 1998;
210 Meir et al., 2002\). Sunfleck penetration through the canopy and the differential effects of direct and diffuse beam
211 radiation on modelled carbon and water exchange in JULES were studied by Mercado et al. \(2009\). This enabled
212 JULES to reproduce the different light-response curves of GPP under diffuse and direct radiation conditions at
213 both a broadleaf and needleleaf temperate forest.](#)

215 **2.2 Physiology Developments**

216 **2.2.1 Farquhar photosynthesis for C_3 plants and parameterisation**

217 We implement the Farquhar photosynthesis scheme (Farquhar et al., 1980) to describe the leaf-level biochemistry
218 of photosynthesis for C_3 vegetation following the approach of Mercado et al. (2018). Here the leaf-level

219 photosynthesis is calculated as the minimum (note no smoothing) of two potentially limiting rates (Equation 1a).
 220 These two rates are i) Rubisco-limited photosynthesis (Equation 2) and ii) light-limited photosynthesis with a
 221 dependence on the incident photosynthetically active photon flux density and the potential electron transport rate
 222 (Equations 3 and 4). Note, as in the original Farquhar formulation, we do not include a TPU-limited (triose
 223 phosphate utilisation) rate. Further, recent empirical studies suggest that TPU limitation rarely limits
 224 photosynthesis under present-day CO₂ concentrations and is also unlikely to limit photosynthesis at elevated CO₂
 225 (Kumarathunge et al., 2019a). This, and the current uncertainty in the formulation of TPU limitation of
 226 photosynthesis led Rogers et al. (2021) to conclude it is an unnecessary complication in LSMs. Hence:

$$227 \quad A_p = \min\{A_v, A_j\} - R_d \quad (1a)$$

$$228 \quad A_n = A_p \beta \quad (1b)$$

229 where A_p is the net potential (i.e. unstressed) leaf photosynthetic carbon uptake (mol m² s⁻¹), R_d is the rate of leaf
 230 respiration in the dark (mol m² s⁻¹), A_n is the net photosynthetic rate (mol m² s⁻¹) which accounts for the impact of
 231 soil moisture stress on photosynthetic rate by multiplying A_p by the soil water stress factor β . Rubisco-limited
 232 photosynthesis (A_v , mol m² s⁻¹) is calculated as in Equation 2. The maximum rate of carboxylation of Rubisco is
 233 determined by V_{cmax} (mol m² s⁻¹), c_i and o_a are the intercellular concentrations of CO₂ and O₂ (both Pa), K_c and K_o
 234 (both units of Pa) are the Michaelis Menten coefficients for Rubisco carboxylation and oxygenation respectively,
 235 and Γ (Pa) is the CO₂ compensation point in the absence of mitochondrial respiration.

236

$$237 \quad A_v = \frac{V_{cmax} (c_i - \Gamma)}{[c_i + K_c \left(1 + \frac{o_a}{K_o}\right)]} \quad (2)$$

238 The light-limited rate of photosynthesis (A_j , mol m² s⁻¹) (Equation 3) is a function of the rate of electron transport
 239 J (mol m² s⁻¹) which is represented in Equation 4. J depends on the incident photosynthetically active photon flux
 240 density Q (mol quanta m² s⁻¹), the potential rate of electron transport J_{max} (mol m² s⁻¹), and the apparent quantum
 241 yield of electron transport α (mol electrons mol⁻¹ photon); fixed at 0.3 (mol electrons mol⁻¹ photon) following
 242 Medlyn et al. (2002), and θ a non-rectangular hyperbola smoothing parameter which takes a value of 0.9 (unitless)
 243 following Medlyn et al. (2002). The factor of four used in the Farquhar model in Equation 3 accounts for four
 244 electrons being required per carboxylation/oxygenation reaction.

245

$$246 \quad A_j = \left(\frac{J}{4}\right) \frac{(c_i - \Gamma)}{(c_i + 2\Gamma)} \quad (3)$$

247

$$248 \quad \theta J^2 - (\alpha Q + J_{max})J + \alpha Q J_{max} = 0 \quad (4)$$

249

250 JULES currently uses Q_{10} functions in the Collatz scheme to describe the temperature dependency of V_{cmax} , K_c ,
 251 K_o , and Γ (see Notes S1). In our implementation of the Farquhar scheme, temperature sensitivities for the K_c , K_o ,
 252 and Γ latter parameters are taken from Bernacchi et al. (2001) as described in Medlyn et al. (2002). These are the

Formatted: Font: Italic

Formatted: Font: Italic

Formatted: Font: Italic, Subscript

253 same temperature sensitivities used by experimentalist to derive estimates of photosynthetic capacity parameters
 254 (Rogers et al., 2017). Of particular importance to our analysis here are the temperature responses of V_{cmax} and J_{max} .
 255 Equation 5 describes the temperature response of both parameters:

$$256 \quad k_T = k_{25} \exp \left[H_a \frac{(T_l - T_{ref})}{T_{ref} R T_l} \right] \frac{1 + \exp \left[\frac{T_{ref} \Delta S - H_d}{T_{ref} R} \right]}{1 + \exp \left[\frac{T_l \Delta S - H_d}{T_l R} \right]} \quad (5)$$

257 Here, k_T ($\mu\text{mol m}^{-2} \text{s}^{-1}$) is either V_{cmax} or J_{max} at leaf temperature T_l (K), k_{25} ($\mu\text{mol m}^{-2} \text{s}^{-1}$) is the rate of V_{cmax} or J_{max}
 258 at the reference temperature T_{ref} of 25 °C (298.15 K), R is the universal gas constant ($8.314 \text{ J mol}^{-1} \text{ K}^{-1}$), H_a and
 259 H_d (J mol^{-1}) are the activation and deactivation energies respectively, and ΔS ($\text{J mol}^{-1} \text{ K}^{-1}$) is an entropy term (see
 260 Table 1 for PFT-specific parameter values). Broadly, H_a describes the rate of exponential increase of the function
 261 below the optimum temperature (T_{opt}), and H_d describes the rate of decrease above the T_{opt} . ΔS and T_{opt} are related
 262 by Equation 6, which is used to calculate the T_{opt} of V_{cmax} and J_{max} (Table 1):

$$264 \quad T_{opt} = \frac{H_d}{\Delta S - R \ln \left[\frac{H_a}{H_d - H_a} \right]} \quad (6)$$

266 **Table 1.** PFT-specific parameters for the required temperature dependency of V_{cmax} and J_{max} in the Collatz and
 267 Farquhar photosynthesis schemes. PFT codes (left column) are BET-tr: Broadleaf evergreen tropical tree, BET-
 268 te: Broadleaf evergreen temperate tree, BDT: Broadleaf deciduous tree, NET: Needle leaf evergreen tree, NDT:
 269 Needle leaf deciduous tree, C₃: C₃ grass, C₄: C₄ grass, ESH: Evergreen shrub, DSH: Deciduous shrub.

	Collatz			Farquhar					H_d or H_d H_d	
	T_{upp}	T_{low}	$T_{opt,vcmax}$	$H_{a,vcmax}$	$H_{a,jmax}$	ΔS_{vcmax}	ΔS_{jmax}	$T_{opt,vcmax}$		$T_{opt,jmax}$
	(°C)	(°C)	(°C)	(J mol ⁻¹)	(J mol ⁻¹)	(J mol ⁻¹ K ⁻¹)	(J mol ⁻¹ K ⁻¹)	(°C)		(°C)
BET-tr	43	13	39.00	86900	64000	631	635	42.71	38.73	200000
BET-te	43	13	39.00	59600	35900	634	632	38.80	37.10	200000
BDT	43	5	39.00	49300	38800	658	663	26.57	23.22	200000
NET	37	5	33.00	63100	36400	642	643	35.28	31.96	200000
NDT	36	-5	34.00	49300	38800	658	663	26.57	23.22	200000
C ₃	32	10	28.00	97200	112000	660	663	28.00	28.00	199000
C ₄	45	13	41.00	-	-	-	-	-	-	-
ESH	36	10	32.00	59600	35900	634	632	38.80	37.10	200000
DSH	36	0	32.00	49300	38800	658	663	26.57	23.22	200000

271

272

273

Formatted: Superscript

274 To find new estimates for V_{cmax} and the $J_{max}:V_{cmax}$ ratio at T_{ref} of 25°C for use with the Farquhar model for the 9
 275 PFT's in JULES we used the global dataset from Walker et al. (2014) which includes data from 356 species. For
 276 V_{cmax} and J_{max} , Walker et al. (2014) re-analysed the data to remove the variation in these two parameters across
 277 studies caused by different parametric assumptions used in their derivation from $A-C_i$ curves (e.g. using a common
 278 set of kinetic parameters, and reporting values at 25°C). We calculated the mean V_{cmax} and J_{max} across studies
 279 conducted at ambient CO₂ concentration for each of the JULES PFTs (Table 2). To parameterise the deciduous
 280 needleleaf tree (NDT) PFT, we use the values for the evergreen needleleaf tree (NET) PFT because the data for
 281 NDT was from a single study on one juvenile (3 years old) species. An exception was the tropical broadleaf
 282 evergreen tree (BET-tr) PFT, where we use V_{cmax} and J_{max} from the dataset collated in the more recent compilation
 283 by Kumarathunge et al. (2019b), as this study includes many more tropical tree species than any previous meta-
 284 analysis.

285 Parameter values for the temperature response functions for V_{cmax} and J_{max} (Equation 5) in the Farquhar scheme
 286 were taken from a global dataset of photosynthetic CO₂ response curves, which entrained data from 141 C₃
 287 species, ranging from the tropical rainforest to Arctic tundra (Kumarathunge et al., 2019b). The study provides
 288 parameter values for tree PFT's that match those in JULES, e.g. tropical broadleaf evergreen trees (BET-tr PFT
 289 in JULES), temperate broadleaf evergreen trees (BET-te), broadleaf deciduous trees (BDT) and needleleaf
 290 evergreen trees (NET). For the remaining JULES PFTs, BDT values are used for NDT and deciduous shrubs
 291 (DSH), and BET-te values are used for evergreen shrubs (ESH). Kumarathunge et al. (2019b) do not include data
 292 for C₃ grasses, therefore to parameterise the temperature dependency of V_{cmax} and J_{max} for this PFT, we fitted both
 293 to the existing V_{cmax} temperature response function in the Collatz scheme for C₃ grasses because of a scarcity of
 294 data in the literature. Fig. S1 shows the temperature dependency of V_{cmax} , J_{max} and gross photosynthesis for Collatz
 295 and Farquhar using the PFT-specific parameters in Table 1 and Table 2.

296

297 **Table 2.** PFT-specific parameters for the Collatz and Farquhar photosynthesis schemes.

298

	Collatz		Farquhar			
	V_{cmax25} ($\mu\text{mol m}^{-2}\text{s}^{-1}$)	α (intrinsic) ($\text{mol CO}_2 \text{ mol}^{-1}$ PAR)	V_{cmax25} ($\mu\text{mol m}^{-2}\text{s}^{-1}$)	J_{max25} ($\mu\text{mol m}^{-2}\text{s}^{-1}$)	$J_{max}:V_{cmax}$	α (apparent) ($\text{mol electrons mol}^{-1}$ photon)
BET-tr	41.16	0.08	39.50	63.20	1.60	0.30
BET-te	61.28	0.06	68.95	112.59	1.63	0.30
BDT	57.25	0.08	55.24	98.30	1.78	0.30
NET	53.55	0.08	50.80	75.14	1.48	0.30
NDT	50.83	0.10	50.80	75.14	1.48	0.30
C ₃	51.09	0.06	43.83	108.07	2.47	0.30
C ₄	31.71	0.04	-	-	-	-
ESH	62.41	0.06	68.96	112.59	1.63	0.30
DSH	50.40	0.08	55.24	98.30	1.78	0.30

299

300 2.2.2 Medlyn model of g_s and parameterisation

301 In JULES, g_s (m s^{-1}) is represented in Equation 7.

$$302 \quad g_s = 1.6RT_l \frac{A_n}{c_a - c_i} \quad (7)$$

303 where the factor 1.6 accounts for g_s being the conductance for water vapour rather than CO_2 , R is the universal
304 gas constant ($\text{J K}^{-1}\text{-mol}^{-1} \text{K}^{-1}$), T_l is the leaf surface temperature (K), c_a and c_i (both Pa) are the leaf surface and
305 internal CO_2 partial pressures respectively, and A_n is the net photosynthetic rate. Here, c_i is unknown and is
306 calculated in JULES using the Jacobs scheme as in Equation 8, and relates the ratio of ambient (c_a) to leaf
307 intercellular (c_i) partial pressure of CO_2 (c_i/c_a), to leaf humidity deficit:

$$308 \quad c_i = (c_a - \Gamma)f_0 \left(1 - \frac{d_q}{dq_{crit}}\right) + \Gamma \quad (8)$$

309 where Γ (Pa) is the CO_2 photorespiration compensation point, d_q is the humidity deficit at the leaf surface (kg kg^{-1})
310 ¹), and dq_{crit} (kg kg^{-1}) and f_0 are PFT specific parameters representing the critical humidity deficit at the leaf surface
311 and the leaf internal to atmospheric CO_2 ratio (c_i/c_a) at the leaf specific humidity deficit (Best et al., 2011). To
312 implement the Medlyn model, Equation 9 is used to calculate c_i , retaining Equation 7 to calculate g_s . In Equation
313 9, g_l ($\text{kPa}^{0.5}$) is a PFT-specific model parameter and d_q is expressed in kPa. The Medlyn scheme is based on
314 optimisation theory, and so assumes that stomatal aperture is regulated to maximize carbon gain while
315 simultaneously minimising water loss:

$$316 \quad c_i = c_a \left(\frac{g_l}{g_l + \sqrt{d_q}}\right) \quad (9)$$

317 PFT-specific values of the g_l parameter were derived for the nine JULES PFTs from the global data base of Lin
318 et al. (2015) (Table 3). The g_l parameter represents the sensitivity of g_s to the assimilation rate, i.e. plant water
319 use efficiency, and was derived as in Lin et al. (2015), by fitting the Medlyn et al. (2011) model to observations
320 of g_s , photosynthesis, and VPD, assuming an intercept of zero. A non-linear mixed-effects model was used to
321 estimate the model slope coefficient, g_l , for each PFT, where individual species were assumed to be the random
322 effect to account for the differences in the g_l slope among species within the same group, following Lin et al.
323 (2015).

Formatted: Font: Italic

Formatted: Font: Italic

332 **Table 3.** PFT-specific parameters required for the Jacobs and Medlyn g_s schemes.

333

	Jacobs f_o	Jacobs dq_{crit} (kg kg^{-1})	Medlyn $g1$ ($\text{kPa}^{0.5}$)
BET-tr	0.875	0.090	5.31
BET-te	0.892	0.090	3.37
BDT	0.875	0.090	4.45
NET	0.875	0.060	2.35
NDT	0.936	0.041	2.35
C ₃	0.931	0.051	5.25
C ₄	0.800	0.075	1.62
ESH	0.950	0.037	3.29
DSH	0.950	0.030	5.47

334

335 2.2.3 Thermal acclimation of photosynthetic capacity

336 The Kattge and Knorr (2007) acclimation algorithm (“AcKK”) is based on the parameters of the Farquhar
 337 photosynthesis scheme, hence acclimation is implemented in the Farquhar model. The AcKK algorithm uses
 338 empirical relationships to describe the response of V_{cmax} , J_{max} , and the $J_{max}:V_{cmax}$ ratio to changes in T_{growth} (defined
 339 in AcKK as the average temperature (day and night) of the previous 30 days), and importantly it represents
 340 combined acclimation and adaptation processes. Kattge and Knorr (2007) found that ΔS_v , ΔS_j , and the $J_{max}:V_{cmax}$
 341 ratio decrease linearly with increasing T_{growth} following Equation 10. This means according to these relationships,
 342 the optimum temperatures (T_{opr}) of V_{cmax} and J_{max} (T_{oprV} and T_{oprJ}) increase by 0.44°C and 0.33°C per degree increase
 343 in T_{growth} respectively, and the $J_{max}:V_{cmax}$ ratio at 25°C decreases by 0.035°C per degree increase in T_{growth} .

$$344 \quad x_i = a_i + b_i T_{growth} \quad (10)$$

345 The x is either ΔS_v , ΔS_j or the $J_{max}:V_{cmax}$ ratio, and the sub-index i refers to the parameter values (a and b shown in
 346 Table 4) for V_{cmax} , J_{max} or the $J_{max}:V_{cmax}$ ratio. T_{growth} is the growth temperature (calculated online as the mean
 347 temperature of the previous 30 days).

348

349 **Table 4.** Parameter values derived by Kattge & Knorr (2007) and used in this study in Equation 10 to model
 350 thermal acclimation of photosynthesis using the AcKK scheme.

	Acclimation	
	a	b
ΔS_j	659.7	-0.75
ΔS_v	668.39	-1.07
$J_{max}:V_{cmax}$	2.59	-0.035

351 3. Model evaluation and application

352 3.1 Site level simulations

353 JULES was applied using four model configurations (Table 5) with observed meteorology, and evaluated against
354 data from 17 eddy covariance sites (Table S1, Fig. S2). This collection of eddy covariance measurements
355 represents a range of climates and land cover types (Table S1, Fig. S2). In all simulations the vegetation cover
356 was prescribed, removing any biases that the modelled competition may introduce through self-diagnosis of PFT
357 extents. Prescribed leaf area index (*LAI*) was used where site data was available, otherwise the JULES phenology
358 scheme was switched on allowing the model to evolve the *LAI*. Model output was evaluated against fluxes of
359 gross primary productivity (GPP) and evaporative fraction (EF). We used EF rather than latent heat flux to
360 minimise issues with incomplete closure of the energy balance (that can typically range from 5 to 30 % at some
361 eddy covariance sites, Liu et al. (2006)). For analysis we used daytime values only (i.e. where the shortwave
362 radiation was $> 10 \text{ W m}^{-2}$) from days with no missing data, and compare mean seasonal diurnal cycles of modelled
363 GPP and EF against the observed fluxes. The mean seasonal cycle calculated over the entire measurement period
364 is used in order to assess the mean model behaviour.

365 We evaluate the site-level simulations with RMSE (root mean square error) for the seasonal diurnal cycle of
366 simulated (daytime) fluxes (GPP and EF). For each site, the time period of the simulation and therefore evaluation
367 period is stated in Table S1. We summarise the changes in RMSE using the relative improvement for each model
368 configuration (*i*) compared to the current standard JULES configuration of Collatz with Jacobs (Clz.Jac). The
369 statistic is calculated so that positive values show an improvement compared to Clz.Jac and therefore a better
370 comparison to the observations:

$$371 \text{RMSE}_{rel_i} = \frac{\text{RMSE}_{Clz.Jac} - \text{RMSE}_i}{\text{RMSE}_{Clz.Jac}} \quad (11)$$

372

373

374

375

376

377

378

379

380

381

382 **Table 5.** Description of the four model experiments performed both at site level and globally, with the JULES
 383 land surface model.

384

Model simulation	Description	Photosynthesis scheme	Stomatal closure	Temperature dependency of photosynthesis	T_{growth}
Clz.Jac	The original photosynthesis and stomatal conductance (g_s) schemes used in JULES.	Collatz <i>et al.</i> , (1991)	Jacobs (1994)	Q_{10} function for K_c , K_o , Γ and V_{cmax} (PFT specific). T_{opt} varies by PFT but is fixed spatially and temporally.	NA
Fq.Jac	The Farquhar photosynthesis scheme is implemented with updated V_{cmax} and J_{max} values, and updated parameters for the temperature response of photosynthesis (ΔS and H_a for V_{cmax} and J_{max}) with original g_s scheme used in JULES.	Farquhar <i>et al.</i> , (1980)	Jacobs (1994)	Arrhenius function for K_c , K_o , Γ , V_{cmax} and J_{max} (latter two both PFT specific). T_{opt} varies by PFT but is fixed spatially and temporally.	NA
Fq.Med	The Medlyn stomatal closure is implemented with the parameter g_l that varies by PFT with Farquhar photosynthesis model implementation.	Farquhar <i>et al.</i> , (1980)	Medlyn <i>et al.</i> , (2011)	Arrhenius function for K_c , K_o , Γ , V_{cmax} and J_{max} (latter two both PFT specific). T_{opt} varies by PFT but is fixed spatially and temporally.	NA
AcKK.Med	Thermal acclimation of photosynthetic capacity accounted for. Implemented within the Farquhar model coupled to the Medlyn g_s model.	Farquhar <i>et al.</i> , (1980)	Medlyn <i>et al.</i> , (2011)	Arrhenius function for K_c , K_o , Γ . Thermal acclimation of photosynthetic capacity implemented following Kattge & Knorr (2007). Parameters describing the temperature sensitivity of photosynthesis (ΔS for V_{cmax} and J_{max} , and the $J_{max}:V_{cmax}$) allowed to acclimate to the temperature of the growth environment (T_{growth}). T_{opt} adjusts to changes in T_{growth} so varies spatially and temporally.	Yes

385

386 3.2 Global scale simulations

387 Four JULES simulations were performed globally for the period 1979-2013 as outlined in Table 5. These global
 388 present-day simulations were run at $0.5^\circ \times 0.5^\circ$ spatial resolution. The WFDEI meteorological dataset was used to
 389 drive the model (Weedon *et al.*, 2014). This has a three hour temporal resolution that JULES interpolated down
 390 to an hourly model time step. To focus on the direct effects of the model changes on GPP and surface energy
 391 fluxes, the land surface properties of the model were prescribed. We use a static map of land cover (in terms of

392 different PFT extents) derived from the European Space Agency's Land Cover Climate Change Initiative (ESA
393 LC_CCI) global vegetation distribution version 1.6 for the 2010 epoch (Poulter et al., 2015) (Fig. S3) following
394 that used in Harper et al. (2016). Seasonally varying LAI_t were derived from the Global Land Surface Satellite
395 (GLASS) dataset (Xiao et al., 2016). Prescribed parameters were used for the hydraulic and thermal properties of
396 the soil from a modified version of the H1 lookup-table from Zhang and Schaap (2017) that depends upon the soil
397 textural type from SoilGrids (Hengl et al., 2014). We also prescribe transient atmospheric CO₂ concentrations
398 based on annual mean observations from Mauna Loa (Tans and Keeling, 2014). A spin-up of 80 years was
399 performed (re-cycling through the period 1979 to 1999), which is sufficient to equilibrate soil temperature and
400 soil moisture.

Formatted: Font:

401 The global offline present-day simulations were compared against the global evaluation products, and for both
402 model output and observations we calculate seasonal means over the period 2002 to 2012. We used the global
403 FluxCom product to evaluate modelled GPP, LE, H and ET (Jung et al., 2020; Tramontana et al., 2016). We
404 compare our simulations against the FluxCom ensemble product (RS+MET) driven with the same forcing
405 (WFDEI), as is recommended by Jung et al. (2019) to minimise deviations due to different climate input data. To
406 convert LE to ET we assume a constant latent heat of vaporization of 2.5 MJ mm⁻¹. We also use the model derived
407 product from GLEAM-v3.3a to evaluate ET, and additionally use the MODIS GPP product (Zhao et al., 2005;
408 Zhao and Running, 2010; Zhao et al., 2006) to evaluate simulated global GPP.

409 Global future climate simulations were performed forced with meteorological output (1960 to 2050) from the
410 HadGEM3-GC3.1 model atmosphere-only simulations at 3 hour temporal resolution and N512 spatial resolution
411 (Roberts et al., 2019; Williams et al., 2018). These projections follow the CMIP6 HighResMIP protocol (Haarsma
412 et al., 2016). This choice of forcing to drive JULES is to allow comparison of the offline runs performed in this
413 study with the equivalent simulations currently being undertaken in the coupled HadGEM3-GC3.1 model to
414 explore land-atmosphere feedbacks arising from changes implemented to the plant physiology routines in this
415 work. The factorial set of offline simulations in this work provide a systematic sensitivity study that is less
416 computationally expensive with which to help understand behaviour seen in the coupled model. The output at
417 N512 was re-gridded to 0.5° x 0.5° using conservative interpolation which ensures the physical conservation of
418 each variable. Fig. S4 shows the mean temperature and precipitation change by region over the study period, and
419 the atmospheric CO₂ concentration. Atmospheric CO₂ concentrations were prescribed based on observations up
420 to 2014 as described in historical CMIP6 simulations (Eyring et al., 2016). From 2015 onwards, atmospheric CO₂
421 concentrations were based on a high-end emission scenario of the Shared Socioeconomic Pathways (SSP5) with
422 the Representative Concentration Pathway 8.5 (RCP8.5) (Haarsma et al., 2016). As for the current-day
423 simulations, LAI_t and land cover and soil properties were prescribed using the same datasets. A spin-up period of
424 80 years (re-cycling through the period 1960 to 1980) was again used to equilibrate soil temperature and soil
425 moisture.

426 We analyse the future global simulations using the 'difference of difference' approach. This method explicitly
427 targets the change in the variable of interest over the study period resulting from the change in process alone, and
428 negates differences that may arise from different initial starting points of each simulation (different initial
429 conditions):

430 $Effect = (\bar{X}_{2050} - \bar{X}_{1980}) - (\bar{Y}_{2050} - \bar{Y}_{1980})$ (12)

431 where X and Y represents the simulation with the process of interest and Y represents the simulation with the
 432 alternative representation without the process respectively, and 2050 and 1980 represent the end and start of the
 433 simulation analysis period respectively (calculated as the mean over 2040 to 2050, and 1980 to 1990 respectively).
 434 For example, to look at the impact of changing photosynthesis schemes, $X = Fq.Jac$ and $Y = Clz.Jac$. In this case,
 435 both configurations are using the Jacobs g_s scheme, only the photosynthesis scheme changes from Collatz to
 436 Farquhar. The impact of changing g_s scheme is assessed where $X = Fq.Med$ and $Y = Fq.Jac$. The impact of thermal
 437 acclimation is assessed where $X = AcKK.Med$ and $Y = Fq.Med$, here both simulations use the Farquhar
 438 photosynthesis scheme and the Medlyn g_s scheme, but X has the addition of thermal acclimation of photosynthesis.

439

440 **4. Results**

441 **4.1 Site level evaluation**

442 Results from the FLUXNET sites comparing the mean seasonal diurnal cycles of GPP and EF against observed
 443 fluxes are summarised in Fig. 1, where reds and yellows indicate reduced RMSE relative to the 'standard' JULES
 444 configuration of Collatz with Jacobs (Clz.Jac), and therefore closer agreement to site level FLUXNET
 445 observations. Results are variable by site and season (Fig. 1, Fig. S543 and Fig. S644), some of which will be due
 446 to other site-specific characteristics that are not simulated well by the model, such as LAI for those sites that rely
 447 on model derived estimates. On the other hand, soil properties are prescribed by parameters that describe the
 448 thermal and hydraulic characteristics of the soil, uncertainties in these parameterisations have consequences for
 449 the simulated soil moisture content at each site, for example, which impacts simulated carbon and water fluxes.
 450 We first consider results for the five tropical sites. Results are mixed for the simulated seasonal diurnal cycle of
 451 GPP at the tropical (EBF / BET-tr) sites, GPP is improved (reduced) with the new JULES model configurations
 452 at three out of the five tropical sites in March-April-May (MAM; Fig. 1a, Fig. S543), with thermal acclimation
 453 leading to the greatest improvements. However in June-July-August (JJA; Fig. 1b, Fig. S543), this improvement
 454 is only found at two of the tropical sites. At the EBF sites, implementing the Farquhar photosynthesis model
 455 means V_{max} is lower (BET-tr, Table 2), and this in addition to the change in temperature sensitivity (Table 1; Fig.
 456 S1a-c), and model structural changes from Collatz to Farquhar results in lower simulated GPP compared to
 457 Collatz. Thermal acclimation allows further adjustments of the T_{optV} , T_{optJ} and the $J_{max} V_{max}$ ratio which results in
 458 lower simulated photosynthesis and therefore GPP compared to Farquhar (Fig. S543). The change from Jacobs g_s
 459 model to Medlyn has minimal impact on simulated GPP for the tropical tree PFT because in both schemes the
 460 modelled c_i has a similar sensitivity to humidity deficit at the leaf surface, with the exception at very low humidity
 461 deficit (Fig. S75; Fig. S543). The simulated seasonal diurnal cycle of EF is improved (reduced) at four out of the
 462 five tropical sites in both MAM and JJA, again with some of the largest improvements seen with thermal
 463 acclimation (Fig. 1c & 1d, Fig. S644).

464 At the C₃ grassland sites (GRA), improved simulated GPP (higher GPP) is seen across all sites in JJA with the
 465 Medlyn g_s scheme and thermal acclimation (Fig. 1b, Fig. S543). This is matched by improvements in simulated
 466 EF (higher EF) across all grassland sites in both seasons, with the exception of US_var in JJA (Fig. 1c & 1d; Fig.

Formatted: Font: Italic

Formatted: Font: 10 pt

Formatted: Font: Italic

Formatted: Font: Italic, Subscript

Formatted: Font: Italic

Formatted: Font: Italic, Subscript

Formatted: Subscript

Formatted: Font: Italic

Formatted: Font: Italic

Formatted: Font: Italic

Formatted: Font: Italic, Subscript

Formatted: Subscript

Formatted: Font: Italic

Formatted: Not Superscript/ Subscript

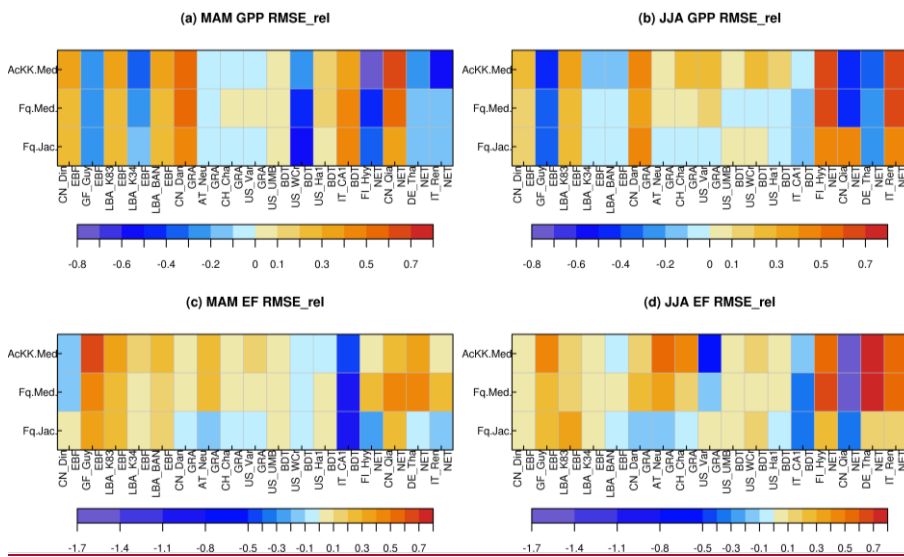
467 [S614](#)). The change from Collatz to Farquhar at the GRA sites means a lower V_{cmax} is used (C3, Table 2) although
468 the temperature sensitivity is similar (Table 1, Fig. S1p, q), this results in lower GPP simulated by Farquhar
469 compared to Collatz which compares worse to the observations (GPP and EF, Fig. 1, [Fig. S513](#)). In contrast to
470 using Farquhar with the Jacobs g_s scheme, using Farquhar with the Medlyn scheme improves simulated GPP and
471 EF, both are increased because for the C3 grass PFT as the humidity deficit at the leaf surface increases c_i
472 simulated by Medlyn is less sensitive compared to Jacobs (Fig. S75; [Fig. S513](#)), leading to higher c_i , higher net
473 canopy photosynthesis and GPP, and higher transpiration and LE. These results suggests the Medlyn scheme has
474 a large impact on simulated carbon and water fluxes for the C3 grass PFT in the JULES model. In JJA, the
475 adjustment of the temperature sensitivity of photosynthesis to the T_{growth} by the thermal acclimation scheme tends
476 to increase GPP compared to Farquhar with no acclimation, and this compares better to the observations ([Fig. 1,](#)
477 [Fig. S513](#)).

478 At the broadleaf deciduous tree sites (BDT) simulated GPP is improved with all JULES model configurations in
479 MAM (higher GPP) at three out of the four sites (Fig. 1a). However in JJA improvements are mainly seen with
480 thermal acclimation (lower GPP compared to Fq.Med, Fig. 1b). Medlyn g_s performs worse at all sites in JJA
481 suggesting either the model formulation or parameters are not suitable to correctly capture stomatal behaviour in
482 this season for this PFT (Fig. 1b, [Fig. S513](#)). Compared to Collatz, the Farquhar model for the BDT PFT uses a
483 lower V_{cmax} (Table 2) and has a considerably lower $T_{optV_{cmax}}$ (Table 1; Fig. S1h), which means that at leaf
484 temperatures below $\sim 22^\circ\text{C}$, photosynthesis is higher with the Farquhar model, and above this photosynthesis is
485 lower than Collatz (Fig. S1g). Consequently, warmer temperatures in JJA lead to lower GPP simulated by
486 Farquhar compared to Collatz, and cooler temperatures in MAM result in slightly higher GPP with Farquhar
487 compared to Collatz ([Fig. S513](#)). Using the Medlyn model means simulated c_i is more sensitive to increasing leaf
488 humidity deficit for the BDT PFT (Fig. S75). Medlyn simulates a lower c_i as humidity deficit increases compared
489 to Jacobs which leads to lower GPP and LE, the magnitude of which depends on the local site humidity conditions.
490 In JJA the Medlyn g_s model performs worse at all sites for GPP (Fig. 1b), although improvements in simulated
491 EF are seen in JJA, where both Medlyn and thermal acclimation improve model performance at three out of four
492 BDT sites (Fig. 1d, [Fig. S614](#)).

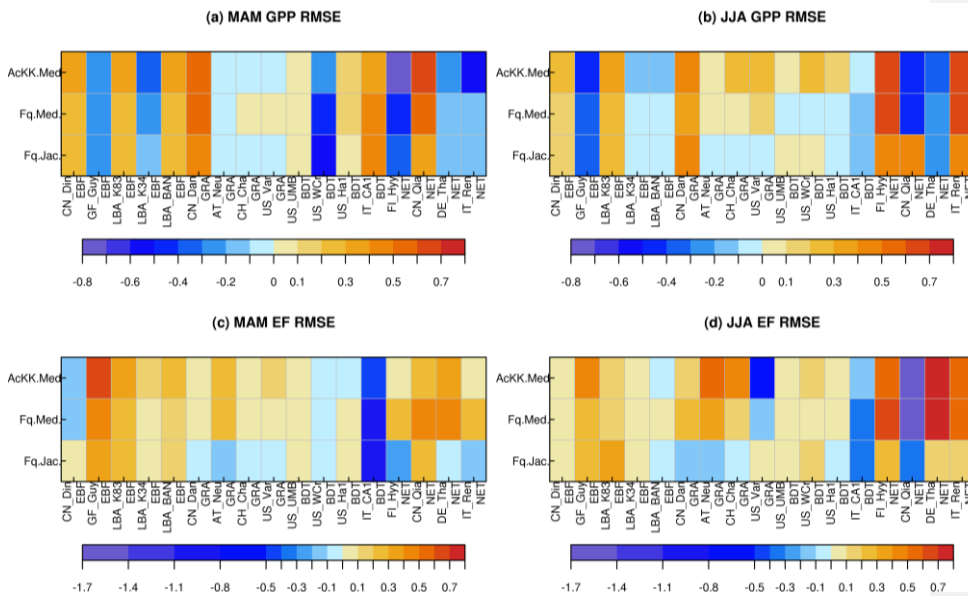
493 At the evergreen needleleaf sites (NET) the most consistent improvements to simulated GPP are seen with the
494 Farquhar model, where simulated GPP in JJA is substantially improved (GPP reduced) at three out of four sites
495 (Fig. 1b, [Fig. S513](#)), in this season both Medlyn and thermal acclimation generate larger improvements in the
496 simulated GPP (reducing GPP further), but this is just at two out of the four sites. In our implementation of the
497 Farquhar model, the NET PFT has a lower V_{cmax} compared to Collatz (Table 2), and a slightly higher $T_{optV_{cmax}}$
498 (Table 1, Fig. S1k). The resulting shape of the temperature response curve for photosynthesis (Fig. S1j) means
499 that at leaf temperatures below $\sim 10^\circ\text{C}$ Farquhar photosynthesis is higher. However above 10°C Farquhar
500 photosynthesis is lower compared to Collatz, resulting in simulated GPP in MAM that tends to be higher with
501 Farquhar than Collatz, and in JJA the opposite occurs ([Fig. S513](#)). In MAM and JJA the Medlyn g_s model
502 simulates some large improvements in EF; c_i simulated by Medlyn is more sensitive to increasing leaf humidity
503 deficit compared to Jacobs (Fig. S75), which results in lower transpiration and EF, and this compares better to the
504 observations ([Fig. 1, Fig. S614](#)).

505

506 **Figure 1.** Relative changes in RMSE for each JULES model configuration compared to Collatz with Jacobs
 507 (Clz.Jac) for hourly daytime a) GPP (March-April-May), b) GPP (June-July-August), c) EF (March-April-May)
 508 and d) EF (June-July-August). Calculated according to equation 11, positive values (Reds and yellows) are where
 509 RMSE is lower compared to the Clz.Jac-JULES configuration, and therefore indicates an improvement ~~with that~~
 510 ~~model configuration~~ compared to the Clz.Jac baseline, and the Fluxnet observations. EBF: Broadleaf evergreen
 511 tropical tree, GRA: C₃ grassland, BDT: Broadleaf deciduous tree, NET: Needle leaf evergreen tree. The fit of each
 512 model configuration to observations and the RMSE are shown in Fig. S543 (GPP) and Fig. S644 (EF).



513



514

515

516

517 **4.2 Global Evaluation**

518 **4.2.1 Spatial differences between model configurations**

519 The impact of changes in the photosynthesis scheme, g_s scheme, adding thermal acclimation of photosynthetic
 520 capacity and the overall change on simulated Figure 2 shows the JJA change in modelled GPP, LE and H are
 521 shown in Figure 2 by comparing with each of the new JULES configurations to the configuration with the
 522 alternative process representation compared to original JULES across the globe. For GPP, the biggest change is
 523 moving from the Collatz photosynthesis scheme to the Farquhar photosynthesis scheme (Fig. 2a). Most notably,
 524 this change results in decreased GPP in the tropical region in JJA of up to $1.5 \text{ gC m}^2 \text{ d}^{-1}$ (up to 10% reduction),
 525 whilst in the high northern latitudes, GPP is increased by up to $1.5 \text{ gC m}^2 \text{ d}^{-1}$ (up to 20% increase). This is
 526 consistent with results from the site-level simulations where GPP was reduced with implementation of the
 527 Farquhar model at tropical sites, and increased in cooler months (MAM) at the evergreen needleleaf forest sites
 528 (here increased GPP in NET dominated areas are in the forests of the high northern latitudes which is consistent
 529 with cooler temperatures). Impacts on LE and H resulting from the move from Collatz to Farquhar are not as
 530 extensive as those seen with GPP (Fig. 2b & 2c). The change from Jacobs g_s scheme to Medlyn impacts LE and
 531 H most, resulting in a pronounced pattern of decreased LE in northern latitudes (up to 10 W m^{-2} , equivalent to a
 532 10% reduction) and corresponding increase in H in JJA (Fig. 2e & 2f). In these JULES simulations, this region is
 533 dominated by NET forest, and the high latitude changes are consistent with results from the site-level simulations,
 534 where using the Medlyn g_s scheme at NET sites resulted in some of the biggest improvements in simulated EF
 535 (lower LE and therefore lower EF). Including thermal acclimation of photosynthesis has the most extensive

Formatted: Font: Italic
 Formatted: Font: Italic, Subscript

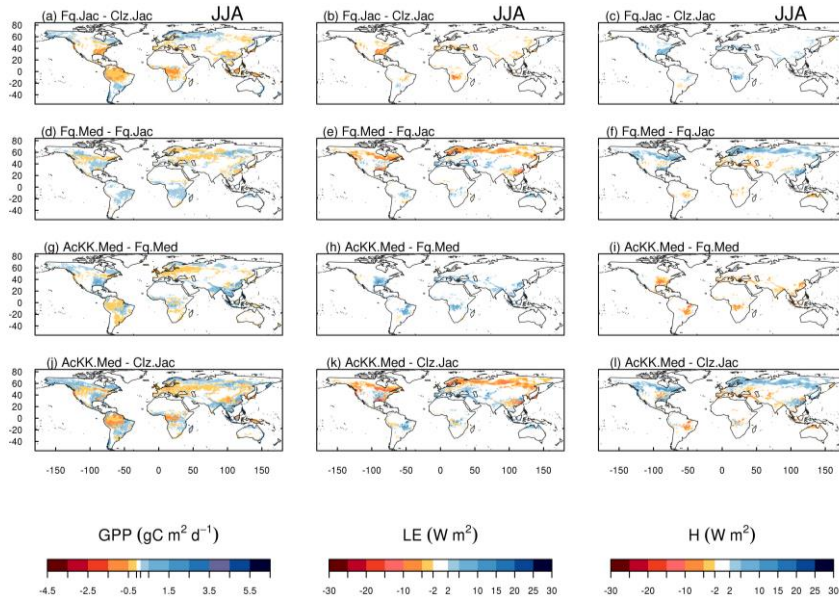
536 impacts on simulated GPP in contrast to LE and H. In the tropical forests GPP is reduced by up to $1 \text{ gC m}^2 \text{ d}^{-1}$
537 (between 2 to 5% reduction) in JJA (Fig. 2g). The impact of acclimation is spatially variable in the temperate
538 region in JJA, with GPP decreased in Europe (between 2 to 5%), but increased in Eastern USA (up to 20%). Some
539 areas of the boreal region see increased GPP (between 2 to 5%). This GPP response demonstrates the impact of
540 thermal acclimation which allows the parameters of the temperature sensitivity functions for photosynthetic
541 capacity (V_{cmax} , J_{max} and $J_{max} \cdot V_{cmax}$) to move in response to the temperature of the growth environment, leading to
542 spatially and temporally different values of the T_{opt} for photosynthesis for each C_3 PFT. Thermal acclimation
543 impacts LE and H to a lesser extent, but where changes are seen, acclimation increases LE with a corresponding
544 decrease in H (Fig. 2h & 2i). Figs. 2j, 2k & 2l show the overall change that results from moving from the traditional
545 JULES set-up of Collatz with Jacobs (Clz.Jac) to Farquhar with thermal acclimation and Medlyn g_s (AcKK.Med),
546 and the impacts on simulated GPP, LE and H can clearly be seen as the trade-off between the dominating effects
547 from each model configuration. For LE and H the response of the simulated energy fluxes is dominated by the
548 change in the representation of g_s , and for GPP the response of simulated carbon fluxes is dominated by the change
549 in the representation of photosynthesis and its response to temperature (i.e. thermal acclimation).

550

551 **Figure 2.** Absolute differences between JULES modelled GPP, latent (LE) and sensible heat (H) for the different
552 JULES model configurations in June-July-August (JJA) to show the impact of a, b, c) changing photosynthesis
553 scheme (Fq.Jac – Clz.Jac); d, e, f) changing g_s scheme (Fq.Med – Fq.Jac); g, h, i) accounting for thermal
554 acclimation of photosynthesis (AcKK.Med – Fq.Med); and j, k, l) the overall change (AcKK.Med – Clz.Jac)
555 under present-day meteorological conditions. For each variable the mean over the period 2002 to 2012 is used.
556 The absolute mean value simulated by each model configuration (JJA) is shown in Fig. S8. DJF is shown in Fig.
557 ure S9 (mean absolute values) and Fig. S10 (absolute difference)6.

Formatted: Font: Italic

Formatted: Font: Italic, Subscript



558

559

560 **4.2.2 Comparison to global estimates: seasonal mean GPP and ET**

561 Evaluation of simulated global mean GPP by season using FluxCom and MOD17 global GPP products is
 562 presented in Fig. 3a and using global ET from both FluxCom and GLEAM is shown in Fig. 3b. The seasonal
 563 means show thermal acclimation compares best to observations (FluxCom) in JJA (AcKK.Med underestimates
 564 GPP by just 4%, whereas Clz.Jac underestimates GPP by 6%; Fig. 3a & Table S2) and MAM (AcKK.Med
 565 underestimates GPP by just 5%, whereas Clz.Jac underestimates GPP by 11%; Fig. 3a & Table S2), and is in
 566 reasonable agreement with FluxCom in DJF (AcKK.Med overestimates GPP by just 2%, whereas Clz.Jac
 567 underestimates GPP by 4%; Fig. 3a & Table S2). All JULES model configurations have a high GPP bias in SON
 568 compared to FluxCom, and in all seasons GPP is overestimated by all model configurations compared to MOD17,
 569 similarly this is largest in SON. For simulated ET, seasonally the model performance is very similar between the
 570 different JULES configurations, however in both SON and DJF Medlyn (Fq.Med) compares better to both
 571 FluxCom and GLEAM, but the differences are very small (Fig. 3b & Table S3).

572

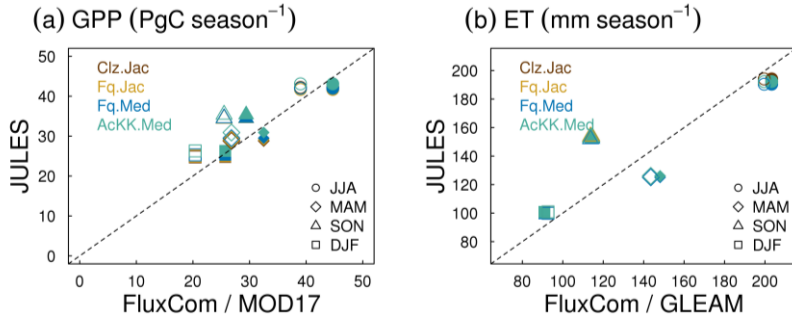
573

574

575

576

577 **Figure 3.** Seasonal mean global a) GPP and b) ET for each JULES model configuration compared to FluxCom
 578 (closed symbols) and MOD17 (GPP) or GLEAM (ET) (open symbols).



579

580

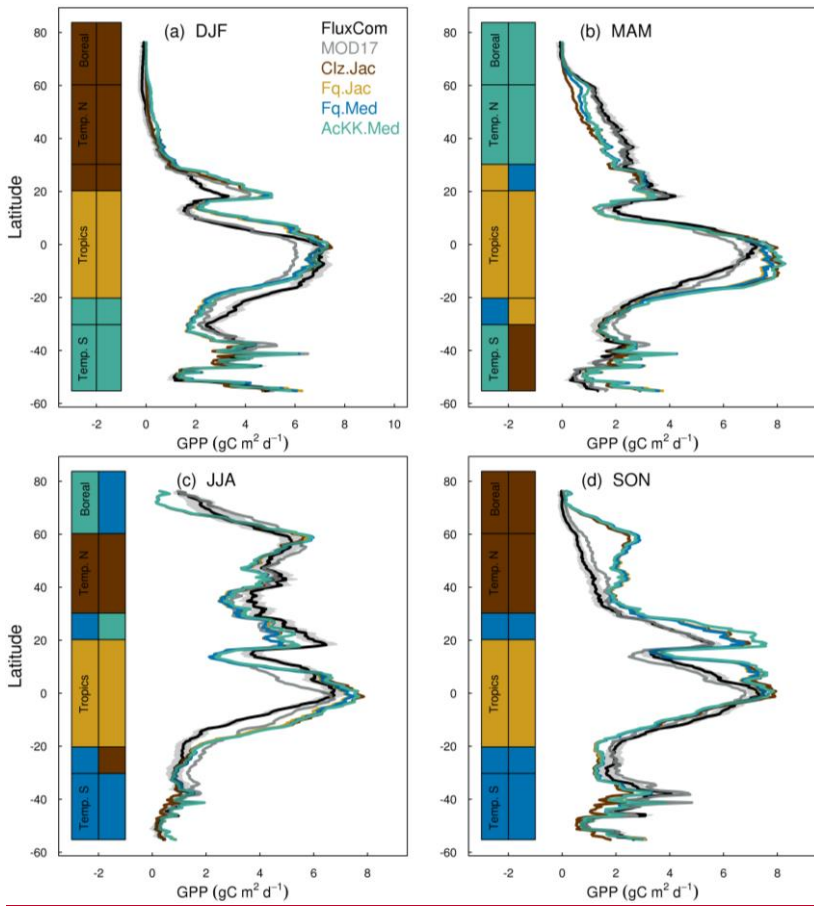
581 4.2.3 Comparison to global estimates: latitudinal mean GPP and ET

582 Figures 4 and 5 present comparisons of seasonal zonal-mean GPP and ET respectively. Firstly, Fig. 4 and Fig. 5
 583 highlight the differences between global products used to evaluate GPP and ET (see e.g. Spafford & MacDougall
 584 2021). For example, FluxCom generally predicts higher GPP in the tropics compared to MOD17, especially in
 585 DJF and MAM, and in JJA the different distribution of GPP by latitude means in the tropics MOD17 GPP is
 586 higher than FluxCom in the southern latitudes, and FluxCom GPP is higher in the northern tropics. Comparison
 587 of the two ET products shows that GLEAM tends to give higher ET in the tropics, particularly in DJF and MAM.
 588 Bearing in mind uncertainties in observation-based estimates of fluxes at this scale we now consider how the
 589 different model configurations compare. Notably, all the JULES model configurations in this study simulate
 590 comparable global carbon and water fluxes for the recent contemporary period and are in reasonable agreement
 591 with the global products used for evaluation. Differences in RMSE between the different model configurations
 592 are small for both GPP and ET. Importantly, the most consistent change is the improvement (lowest RMSE) of
 593 modelled GPP in the tropics with the Farquhar model (Fq.Jac). This improvement is evident in all seasons and
 594 holds when comparing to both FluxCom and MOD17 (Fig. 4). Similarly, estimates of ET are improved in the
 595 tropics (lowest RMSE) with the Farquhar model (Fq.Jac) in DJF and JJA, and with the Medlyn model (Fq.Med)
 596 in MAM and SON, and again this result is not dependent on the choice of observation-based product (Fig. 5).
 597 Another notable change is the improvement of simulated GPP in the temperate north and boreal regions in MAM
 598 with thermal acclimation (AcKK.Med). Deficiencies in the model stand out, but these biases are common to all
 599 model configurations. For example, all configurations simulate an over-prediction of GPP and ET in SON in the
 600 temperate north and boreal regions, overestimated GPP in MAM in tropical southern latitudes (0 to -20°S), under-
 601 predicted GPP and ET in MAM in temperate north and boreal regions, and an over-prediction of ET in MAM in
 602 the temperate and tropical South.

603

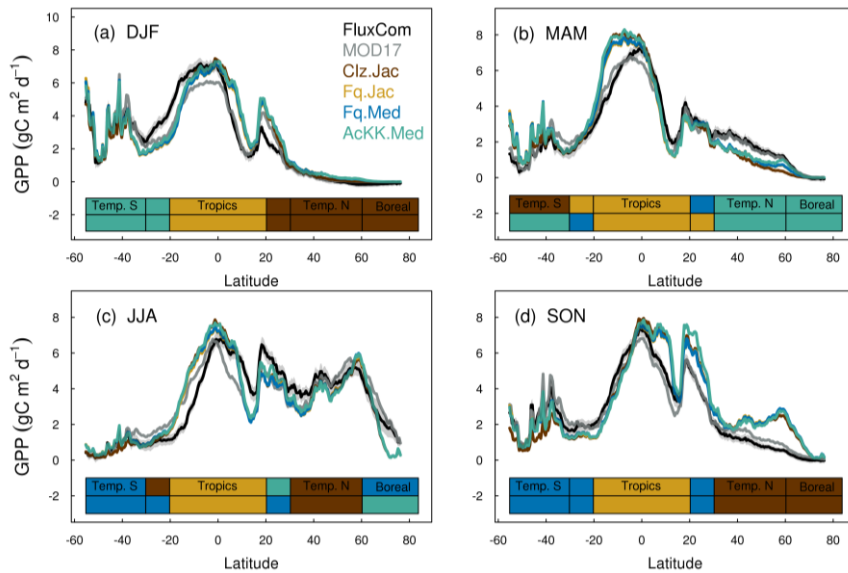
604

605 **Figure 4.** Mean (2002 to 2012) GPP ($\text{g C m}^{-2} \text{d}^{-1}$) by latitude band and season for each JULES model configuration
 606 compared to the FluxCom and MOD17 global GPP products. The bars along the side~~bottom~~ indicate which model
 607 configuration gives the lowest RMSE, and therefore better comparison to FluxCom (right~~hand~~top bar) and
 608 MOD17 (left~~hand~~bottom bar) derived GPP for each region. RMSE values are shown in Tables S4 (FluxCom) and
 609 S5 (MOD17). The grey shaded area shows the uncertainty in the FluxCom GPP product, provided as the median
 610 absolute deviation of ensemble members, this is scaled to a robust estimate of the standard deviation of a normal
 611 distribution by multiplying by 1.4826 according to Jung *et al.*, (2019).



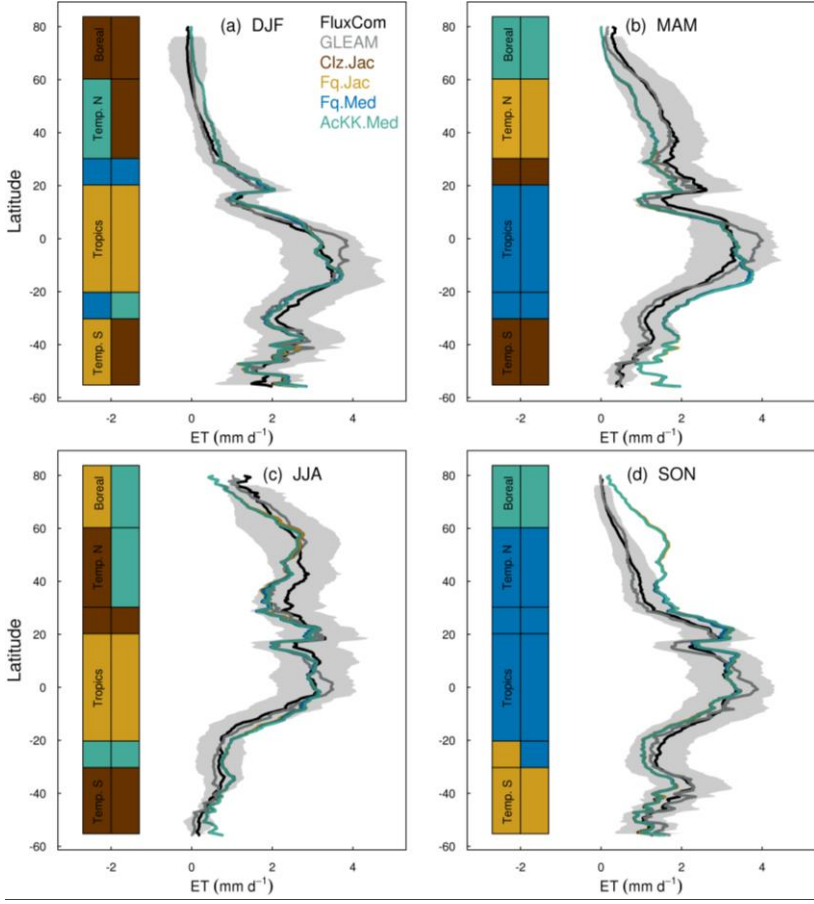
612

613

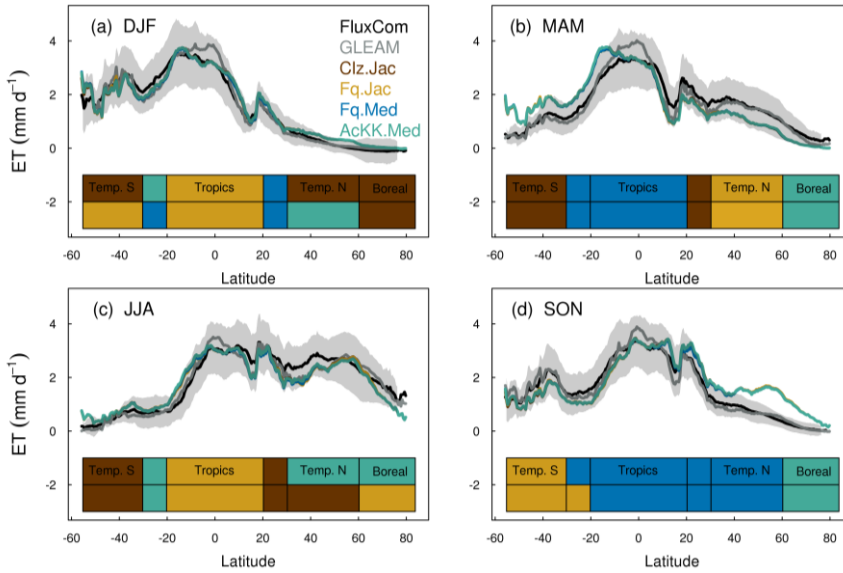


614
615
616

617 **Figure 5.** Mean (2002 to 2012) evapotranspiration (ET mm d⁻¹) by latitude band and season for each JULES
 618 model configuration compared to the FluxCom and GLEAM global ET products. The bars ~~along~~ the ~~side~~~~bottom~~
 619 indicate which model configuration gives the lowest RMSE, and therefore better comparison to FluxCom
 620 (~~right~~~~hand~~~~top~~ bar) and GLEAM (~~left~~~~hand~~~~bottom~~ bar) derived ET for each region. RMSE values are shown in
 621 Table S6 (FluxCom) and Table S7 (GLEAM). The grey shaded area shows the uncertainty in the FluxCom ET
 622 product, provided as the median absolute deviation of ensemble members, this is scaled to a robust estimate of
 623 the standard deviation of a normal distribution by multiplying by 1.4826 according to Jung *et al.*, (2019).



624



625
626

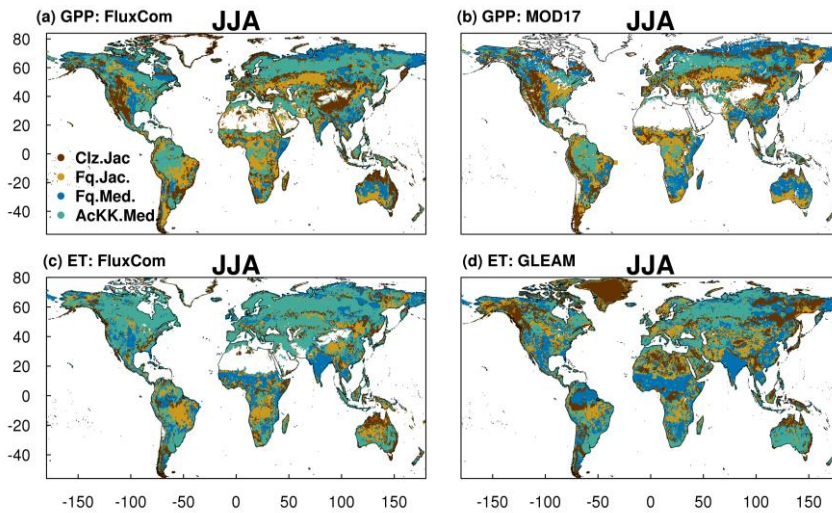
627 **4.2.4 Comparison to global estimates: spatial variability of mean GPP and ET**

628 The spatial variability of simulated GPP and ET is shown in Fig. 6 during JJA (Fig. S117 for DJF). We show
 629 which of the JULES model configurations gives the lowest RMSE compared to observation-based estimates of
 630 GPP and ET from FluxCom, MODIS and GLEAM (actual RMSE in Figs. S128 and S139). The differences in
 631 RMSE are typically small between the different JULES model configurations, however some clear patterns
 632 emerge. Figure 6a & b show that in the tropical forests of the G-e, Amazon basin, and central Africa and Southeast
 633 Asia (Indonesia, Papua New Guinea, Malaysia), in both JJA and DJF (Fig. S117a & b for DJF), GPP simulated
 634 including thermal acclimation (AcKK.Med) compares best to both FluxCom and MOD17 across large spatially
 635 consistent areas. Outside of these areas, Fq.Jac also improves the simulation of GPP in the tropics, as does the
 636 Medlyn g_c model (Fq.Med) in JJA in South China and Indo-China. Also, in the high northern latitudes, dominated
 637 by evergreen needleleaf forests, inclusion of thermal acclimation more closely aligns simulated GPP with both
 638 FluxCom and MOD17 (Fig. 6a & b). Compared to FluxCom, ET in JJA is simulated best by thermal acclimation
 639 (AcKK.Med) in the northern temperate and boreal region, although this pattern is not consistent in comparison to
 640 GLEAM (Fig. 6c & d). In contrast to GPP, results are more mixed in the tropics for ET. In areas dominated by
 641 tropical tree cover, thermal acclimation (AcKK.Med) and Medlyn (Fq.Med) tend to give the lowest RMSE in JJA
 642 and DJF, and in tropical areas dominated by C₃ and C₄ grasses Farquhar (Fq.Jac) performs best (Fig. 6c & d),
 643 although in DJF the Medlyn model gives the lowest RMSE in these areas (Fig. S117c & d). In DJF for both GPP
 644 and ET, in northern temperate and boreal regions the Collatz with Jacobs (Clz.Jac) configuration performs the
 645 best (Fig. S117).

646

Formatted: Font: Italic
Formatted: Font: Italic, Subscript

647 **Figure 6.** Colours indicate the JULES model configuration that gives the lowest RMSE compared to either the a)
 648 FluxCom and b) MOD17 global GPP ($\text{gC m}^{-2} \text{day}^{-1}$) products, or c) FluxCom and d) GLEAM global ET (mm day^{-1})
 649 products for JJA over the period 2002 to 2012. Actual RMSE values shown in Fig. S128 and Fig. S139.



650

651

652 4.3 Application under future climate

653 We run the new configurations forced by variables from a future climate scenario (HadGEM3-GC3.1 forcing
 654 under a high-end emission scenario of the SSPs) to investigate the response of simulated fluxes to long-term
 655 warming. Changing the photosynthesis scheme from Collatz to Farquhar results in lower GPP, (up to 30%
 656 decrease) by 2050 across the high northern latitude forests (Fig. 7a), with the impact on LE (decreased) and H
 657 (increase) less extensive (Fig. 7b & c). This area is dominated by NET, NDT and BDT PFTs in JULES. The
 658 different temperature sensitivity of photosynthesis parameterised with the Farquhar model compared to Collatz
 659 (Fig. S1g, j & m) means at lower leaf temperatures, photosynthesis is higher with Farquhar, however, as leaf
 660 temperature increases, photosynthesis falls in Farquhar relative to Collatz. The crossover point at which this
 661 occurs is relatively low for these PFTs, particularly NET. This impact of the change of temperature sensitivity
 662 was seen in the site-level simulations at FLUXNET NET and BDT sites. There, modelled GPP tended to be higher
 663 with Farquhar than Collatz in MAM, but lower in the warmer conditions of JJA, and in this climate change
 664 scenario the temperate and boreal region both experience large increases in mean annual air temperature (+5°C
 665 from 1980 to 2060, Fig. S4a & c).

666 Replacing the Jacobs g_s scheme with Medlyn has the biggest impact on the surface energy fluxes, with increased
 667 LE of up to 30% and a corresponding decrease in H by 2050 across the temperate region (Fig. 7e & f). This area
 668 is dominated by the C3 grass PFT in JULES which has a less conservative water use strategy in the Medlyn
 669 scheme (high g_l) compared to Jacobs. This means in the Medlyn scheme, the C3 grass PFT is less sensitive to

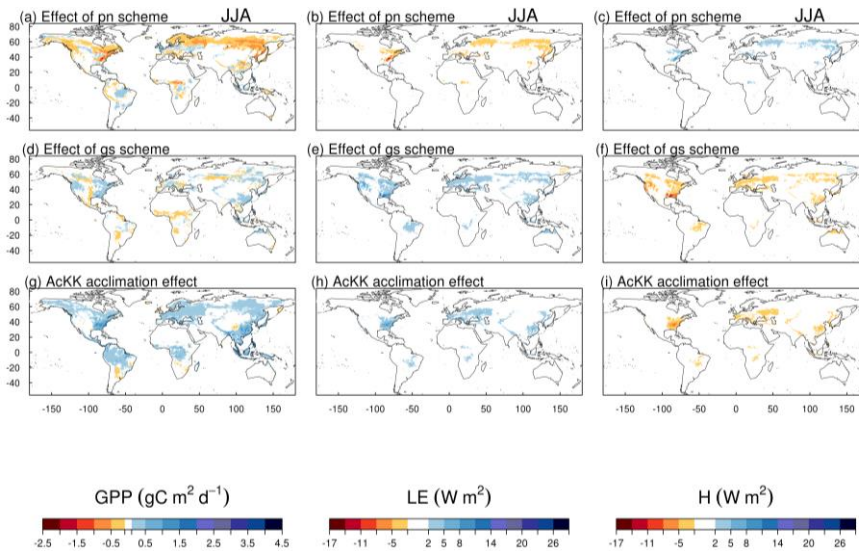
670 increasing humidity deficit at the leaf surface, therefore as humidity deficit increases Medlyn simulates higher c_i
 671 leading to higher rate of transpiration and LE compared to Jacobs (Fig. S75).

672 Thermal acclimation of photosynthesis leads to widespread increases in GPP by 2050 (Fig. 7g). This amounts to
 673 10% in the tropical forests, up to 30% in northern temperate and boreal regions, and up to 40% in south-east Asia.
 674 In this long-term climate change scenario, with large increases in mean annual temperature (Fig. S4), the impact
 675 of thermal acclimation on GPP can clearly be seen. The flexibility in T_{optV} , T_{optJ} and the $J_{max}:V_{cmax}$ ratio of
 676 photosynthesis that thermal acclimation allows through letting these parameters move with the prevailing T_{growth} ,
 677 allows for higher rates of photosynthesis and therefore GPP as temperatures increase. By contrast, in simulations
 678 where photosynthetic rates are controlled by fixed temperature sensitivities, vegetation may have moved past its
 679 thermal optimum. Time series of the area-weighted mean annual GPP show that in this simulation, across the
 680 tropical region, thermal acclimation enhances GPP by ~ 7.5 PgC compared to no acclimation (Fig. 8a). In the
 681 temperate region and sub-tropics thermal acclimation increases GPP by ~ 1 PgC by 2050 (Fig. 8b and d), and in
 682 the boreal region GPP is enhanced by ~ 0.4 PgC (Fig. 8c). Thermal acclimation of photosynthesis also has a large
 683 impact on simulated energy fluxes, most notably in the northern temperate region, where LE is increased by up
 684 to 50 to 60% (decreased H up to 40 to 50%) (Fig. 7h & i).

685

686 **Figure 7.** The difference of difference approach (Equation 12) to determine the impact on GPP ($\text{g C m}^{-2} \text{ day}^{-1}$), LE
 687 and H (both W m^{-2}) of the individual changes to each JULES model configuration over the course of the [future](#)
 688 ([HadGEMGC3.1](#)) simulation (1980 to 2050) in June-July-August (JJA). The AcKK.Med acclimation effect is
 689 calculated from Fig. S16 AcKK.Med – Fq.Med, the effect of the Medlyn g_s scheme is calculated from Fig. S16
 690 Fq.Med – Fq.Jac, and the effect of the photosynthesis scheme is calculated from Fig. S16 Fq.Jac – Clz.Jac.

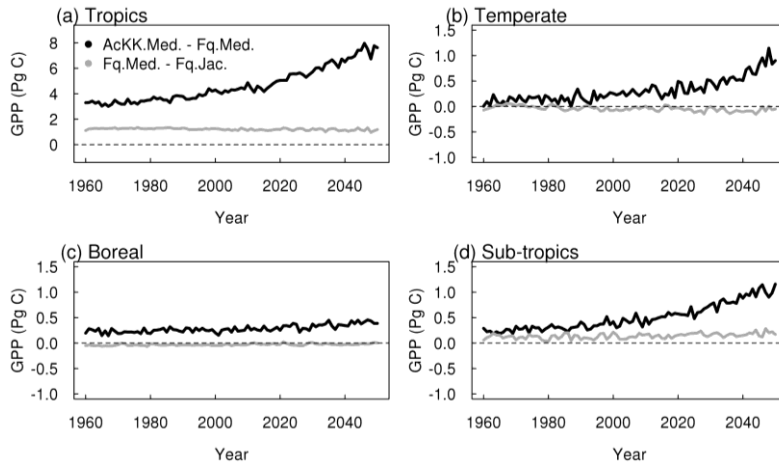
691



692

693

694 **Figure 8.** Time series of the regional mean acclimation effect i.e. AcKK.Med – Fq.Med (black), and the effect of
695 the Medlyn g_s model i.e. Fq.Med – Fq.Jac (grey).



696

697 5. Discussion

698 Photosynthesis and g_s are central to the estimate of carbon and water fluxes in LSMs, and when coupled in ESMs
699 these processes feed-back onto the climate system to influence predictions of future climate change. Therefore
700 improving the representation of these processes in LSMs is important, and previous studies have identified thermal
701 acclimation of photosynthesis as a key missing process (Booth et al., 2012).

702

703 5.1 Performance of the new JULES plant physiology model configurations: Thermal acclimation

704 Our results show that including thermal acclimation of photosynthesis in the JULES model improves simulated
705 carbon and water fluxes in several key areas for the recent contemporary period. Firstly, the seasonal mean
706 estimates of global GPP show that in most seasons (JJA, MAM and DJF) thermal acclimation of photosynthesis
707 with Medlyn g_s (AcKK.Med) predicts GPP in closer agreement with estimates from FluxCom compared to the
708 traditional 'standard' JULES configuration of Collatz photosynthesis with Jacobs g_s (Clz.Jac). Secondly, thermal
709 acclimation with Medlyn g_s improves the simulation of GPP (reduces GPP) in the tropical forests in JJA and DJF
710 (i.e. the Amazon basin and central African rainforest region) and is in closest agreement with estimates of GPP
711 from both FluxCom and MOD17 for these regions. Thirdly, in the high northern latitude forests dominated by
712 evergreen needleleaved trees, thermal acclimation increases GPP in JJA and is again in closest agreement with
713 the observational estimates. Finally, in JJA, AcKK.Med improves the simulation of ET across a large area of the
714 temperate north and boreal regions.

715 Our evaluation therefore suggests that fixed, PFT-specific temperature dependencies for V_{cmax} (and J_{max}) do not
716 accurately simulate GPP for the tropical tree and evergreen needleleaf tree PFTs for the present-day in the JULES

717 model. Thermal acclimation allows the temperature sensitivity of photosynthesis to adjust to the local temperature
718 environment through flexibility in T_{optV} , T_{optJ} and the $J_{max}:V_{cmax}$ ratio. In the tropical forests, for example, GPP is
719 over-estimated by both Clz.Jac and Fq.Jac. The configuration with thermal acclimation reduces GPP compared to
720 both these model configurations. From the leaf-level plots in Fig. S1a, the fixed T_{opt} of photosynthesis in the
721 Collatz scheme is $\sim 33^{\circ}\text{C}$ and in Farquhar is $\sim 34^{\circ}\text{C}$. This is higher than observations from Fig. 1a of Kumarathunge
722 et al. (2019b), where the T_{opt} for net leaf photosynthesis lies between ~ 29 to 32°C , and other studies also show a
723 lower T_{opt} for photosynthesis of around 30°C for mature tropical trees (Hernández et al., 2020; Mau et al., 2018).
724 This supports our results, and suggests the fixed temperature sensitivity of photosynthesis for tropical trees in the
725 JULES model results in a T_{opt} of photosynthesis that is too high for current-day. Thermal acclimation results in a
726 more realistic T_{opt} of photosynthesis for tropical trees because it is influenced by actual growth temperature and
727 so can adjust to local environmental conditions.

728 Under the climate change scenario used in this study, thermal acclimation shows a sustained positive acclimation
729 effect in all regions, increasing GPP in response to long-term warming (although this is less pronounced in the
730 boreal region). By 2050 GPP was $\sim 10\%$ higher with thermal acclimation in the tropical forests, up to 30 to 40%
731 higher across a large area of the northern hemisphere. Our findings broadly agree with Mercado et al. (2018), who
732 implemented the Kattge and Knorr (2007) thermal acclimation scheme into JULES running as part of a coupled
733 climate-carbon model, and found that thermal acclimation increased land carbon storage in tropical and temperate
734 regions. This is in contrast to Lombardozzi et al. (2015) and Smith et al. (2016) whose studies both found a
735 negative impact of photosynthetic thermal acclimation in the tropics, again using the Kattge and Knorr (2007)
736 thermal acclimation scheme. Mercado et al. (2018) attribute these differences to the method used to implement
737 acclimation of the $J_{max}:V_{cmax}$ ratio at 25°C , that is either reducing J_{max} alone as in the case of the latter two studies,
738 or by decreasing J_{max} and increasing V_{cmax} simultaneously whilst keeping the total amount of leaf nitrogen the
739 same as used in the present study and in Mercado et al. (2018). The simulated response of thermal acclimation
740 therefore appears to be sensitive to this subtlety in the parameterisation of the acclimation schemes and warrants
741 further investigation. Yet a clear understanding of what drives the change in the $J_{max}:V_{cmax}$ ratio in response to
742 T_{growth} is still lacking. More recent results from the analysis by Kumarathunge et al. (2019b) highlight the difficulty
743 in pinning down what drives this process. They found that the $J_{max}:V_{cmax}$ ratio responded strongly and consistently
744 to T_{growth} , but whether that was achieved by increasing V_{cmax} , decreasing J_{max} or both was highly variable.

745 The behaviour of the thermal acclimation scheme in JULES in response to long term warming implies unlimited
746 thermal resilience of vegetation, but how realistic is this? Observational studies suggest temperate tree species
747 have sufficient capacity to acclimate to rising temperatures e.g. (Drake et al., 2015; Reich et al., 2018; Sendall et
748 al., 2015), although large inter-specific variability in thermal tolerance is identified in co-occurring temperate tree
749 species (Guha et al., 2018). Studies exploring thermal acclimation of photosynthesis for grasslands and C_3
750 herbaceous vegetation are more limited. For boreal tree species, experimental studies suggest high variability
751 between species with respect to photosynthetic acclimation responses to increasing temperatures, for example,
752 there is an increasing body of work suggesting that the evergreen boreal conifer species *Picea* might be particularly
753 vulnerable to warming (Benomar et al., 2017; Dusenge et al., 2020; Kroner and Way, 2016; Kurepin et al., 2018;
754 Way and Sage, 2008; Zhang et al., 2015). The three year open-air warming experiment of Reich et al. (2018)
755 showed that for 11 temperate and boreal tree species studied, warming increased photosynthesis in most species

Formatted: Not Superscript/ Subscript

Formatted: Not Superscript/ Subscript

Formatted: Not Superscript/ Subscript

756 on wet soils, but not in drier conditions. Further, under moist soil conditions, all deciduous species showed an
757 acclimation response to increased temperatures, however, the two boreal evergreen species, *Abies* and *Picea*,
758 showed no thermal acclimation response at any soil moisture concentration. It is generally thought that evergreen
759 species have a reduced capacity to acclimate growth and photosynthesis to warming compared to deciduous tree
760 species (Dusenge et al., 2020; Way and Yamori, 2014). Therefore, the response of boreal forest ecosystems to
761 warming will depend on species composition given the varied acclimation capacities shown and lower diversity
762 of boreal forests, and, as Reich et al. (2018) highlight, also on interaction with other climate changes such as
763 precipitation. In contrast to temperate and boreal forests, tropical forests are thought to be more susceptible to
764 climate change, having evolved under relatively narrow temperature regimes, and experiencing less seasonal and
765 day-to-day variation in temperature changes (Cunningham and Read, 2003). As a consequence, an increasing
766 number of studies show that tropical trees have less capacity to physiologically acclimate photosynthesis to
767 increasing temperatures (Carter et al., 2021; Dusenge et al., 2021; Mau et al., 2018; Miller et al., 2021; Vårhammar
768 et al., 2015). Other studies have determined high temperature threshold responses of photosynthesis, indicating
769 an ability of tropical trees to acclimate to moderate warming, but more severe warming decreases carbon gain
770 (Doughty and Goulden, 2008; Pau et al., 2018; Slot and Winter, 2017; Sullivan et al., 2020). In two tropical
771 understorey species acclimation of the T_{opt} of photosynthesis was observed in the early successional species,
772 whereas no acclimation capacity was shown by the mid-successional species (Carter et al., 2020). Our study
773 demonstrates a large positive impact of thermal acclimation on GPP in tropical forests. However a notable
774 uncertainty in the parameterisation is that the dataset used in the Kattge and Knorr (2007) scheme to construct the
775 empirical relationships is heavily weighted towards temperate species, including only two boreal species and no
776 tropical species (Kattge and Knorr, 2007). There is a significant gap in understanding tropical forest responses to
777 increasing temperature. Observational studies are starting to address this gap, but this increasing knowledge is yet
778 to be incorporated into models. Therefore, whilst results from this study demonstrate the importance of thermal
779 acclimation of photosynthesis on simulation of the future global carbon cycle, they should be interpreted with
780 some caution. The varied results from experimental studies highlights the research needed to further understand
781 thermal acclimation responses in a variety of ecosystems, over different timescales, and from leaf-level through
782 to canopy, and finally to translate that understanding so it is amenable to incorporation into ESMs.

783 **5.2 Performance of the new JULES plant physiology model configurations: Medlyn g_s**

784 In this study, the Medlyn g_s model had the biggest impact on surface energy fluxes simulated by the C_3 grass PFT
785 and needleleaf evergreen tree PFT in JULES. This reflects a change to the water-use strategy of these PFTs as
786 reported by Lin et al. (2015) that is not currently captured by parameterisations in the JULES Jacobs model. Global
787 simulations with the Medlyn scheme for the recent contemporary period simulated a ~10% decrease in LE
788 (increased H) across the high northern latitudes dominated by the NET PFT compared to the standard JULES
789 Jacobs g_s scheme. The future climate change experiment showed a large response across the temperate region
790 dominated by the C_3 PFT, where LE increased by ~30% (H decreased) with Medlyn. Our study for current-day
791 is in agreement with De Kauwe et al. (2015) who found a large impact of the Medlyn model on transpiration
792 fluxes in needle leaved evergreen trees (~30% reduction) in the CABLE LSM. Coupled simulations using CABLE
793 within the Australian Community Climate and Earth Systems Simulator (ACCESSv1.3b) showed that the Medlyn
794 g_s scheme reduced the LE flux from the land surface over the boreal forests during JJA by 0.5–1.0 mm day⁻¹,

795 leading to warmer daily maximum and minimum temperatures by up to 1.0°C and warmer extreme maximum
796 temperatures by up to 1.5°C (Kala et al., 2015). In future simulations, this new parameterisation of the stomatal
797 scheme in ACCESS1.3 substantially increased the intensity of future heatwaves across Northern Eurasia (Kala et
798 al., 2016).

799 **5.3 Implications for land-atmosphere feedbacks**

800 Modifying the leaf-level stomatal behaviour in JULES impacts the simulated surface energy fluxes. In our study,
801 a change of stomatal opening results from either a direct change in the parameterisation of g_s or through altered
802 stomatal behaviour in response to temperature. In our offline climate change simulation, thermal acclimation
803 increased stomatal opening in response to long term warming, and in some regions this increased the rate of
804 transpiration and evaporative cooling, and decreased the sensible heat flux. When coupled to an atmospheric
805 model, such behaviours have potential to feed-back on the land surface via changes in temperature, cloud cover
806 and precipitation, as for example modelled by De Arellano et al. (2012); Kala et al. (2015); Kala et al. (2016);
807 Kooperman et al. (2018); Zeng et al. (2017). The extent and amplitude of acclimation-induced perturbations to
808 surface energy fluxes in our offline simulation suggests a potential impact on regional scale circulations, for
809 example across the East Asian monsoon region. The impact of these changes to the plant physiology routines in
810 JULES on land-atmosphere feedbacks will be investigated in future work through coupled simulations in the
811 HadGEM global climate model.

812 **5.4 Limitations of this study**

813 Across all latitudes, the changes introduced to JULES by the new plant physiology routines did not degrade the
814 performance of JULES. All model configurations compared reasonably well to the FluxCom and MOD17 GPP
815 products, and FluxCom and GLEAM ET products, given that there are also uncertainties inherent in estimates
816 from these products. For example, the satellite-based products of GPP have recently been shown to incorrectly
817 capture the response of photosynthesis to CO₂, which means they potentially underestimate the response of GPP
818 to rising atmospheric CO₂ (Keenan et al., 2021). Nevertheless, some notable biases in the model were identified
819 that were common to all JULES model configurations, for example the over-prediction of GPP and ET in the
820 temperate and boreal region in SON, and the over-prediction of both fluxes in MAM in the southern tropics (0 to
821 -20°S). Potential sources of error to consider may be the use of a prescribed climatology of MODIS based LAI,
822 which some studies have reported to be inaccurate over forested areas (Shabanov et al., 2005). Other processes
823 currently missing in the model may also contribute to these large biases, such as a lack of seasonality in
824 photosynthetic capacity (i.e. V_{max} and J_{max}) which has been demonstrated for many different forest species (Croft
825 et al., 2017; Wilson et al., 2001), and without which likely causes over-estimation of forest carbon exchange. For
826 example, in SON the high GPP and ET bias occurs in the northern temperate and boreal region which could be
827 linked to a lack of photosynthetic phenology in the model. Towards the end of the growing season leaves in this
828 region have reduced nitrogen content and therefore lower photosynthetic capacity, but because JULES# uses a
829 fixed value for photosynthetic capacity JULES maintains a high rate of carbon assimilation despite having
830 seasonal LAI.

831 More generally, this study revealed limited data to inform the temperature sensitivity response functions of
832 different PFTs for implementation into LSMs. We found only a few datasets for C₃ grass/herbaceous vegetation

833 (e.g. Wohlfahrt *et al.*, (1999) and Joseph *et al.*, (2014)) which represents only limited geographical coverage.
834 Consequently, we fitted the temperature response function for this PFT in the Farquhar scheme to that of the
835 existing function in the JULES Collatz photosynthesis scheme. We also encountered an issue regarding
836 uncertainty about the temperature response functions at low temperatures. The data-led functions we implemented
837 for all PFTs (with the exception of the C3 PFT) from Kumarathunge *et al.* (2019b) showed higher rates of leaf-
838 level photosynthesis at low leaf temperatures compared to the existing functions in the JULES Collatz scheme,
839 where photosynthesis was much lower and goes to zero at 0 °C for most PFTs (see PFT leaf-level temperature
840 sensitivity curves for gross photosynthesis in Fig. S1). In our simulations this led to higher GPP in DJF when
841 using the Farquhar scheme, which increased biases with respect to FluxCom and MOD17 global estimates of
842 GPP. It is desirable to use the temperature response functions from Kumarathunge *et al.* (2019b) as these are
843 entirely data-led. However for some PFTs the resulting behaviour of photosynthesis at very low temperatures
844 looks potentially unrealistic, and the question here is how well constrained by observations are the temperature
845 sensitivity curves at low temperatures? For global modelling applications, understanding the response of
846 photosynthesis to temperature over a wide temperature range is essential, including at low temperatures as well
847 as around the T_{opt} of photosynthesis for different species and PFTs. Additionally, increasing the understanding
848 and data availability of the temperature sensitivity of different species from different biomes will allow greater
849 representation within LSMs of the variation that exists across the globe.

850 The simulations presented in this work use a prescribed map of vegetation cover which means the extent and
851 location of each PFT does not change over time. The model can alternatively be run with dynamic vegetation
852 enabled, which means the model predicts the extent of each PFT, and therefore vegetation cover can change in
853 space and time as PFTs compete with each other in response to changing climatic conditions. Yet to be explored
854 as part of this work, is how changes to the plant physiology routines, as implemented here, might affect the extent
855 of different PFTs over time when vegetation dynamics is enabled. For example, changes to the temperature
856 response of photosynthesis may lead to a competitive advantage of one PFT over another, and therefore the
857 vegetation distribution may be very different as temperatures rise compared to simulations that either use the
858 original Collatz temperature sensitivities or do not include thermal acclimation of photosynthesis. We hypothesise,
859 for example, that allowing thermal acclimation of the temperature sensitivity of photosynthesis would make the
860 vegetation distribution more stable in a warmer climate as vegetation can adjust its photosynthetic capacity to
861 function more efficiently as temperatures rise. Applied in a coupled ESM, a change in vegetation distribution
862 would impact projections of future climate change.

863 The treatment of soil moisture stress in JULES is through a linear response function (the β function, Eq. 12 in
864 Best *et al.*, 2011), the use of which in JULES and other LSMs has been identified as a key source of uncertainty
865 (Blyth *et al.*, 2011; Verhoef and Egea, 2014; Vidale *et al.*, 2021). Incorrect representation of soil moisture stress
866 has large impacts for modelled carbon and water fluxes, and is of particular importance as droughts are predicted
867 to increase in frequency or intensity in the future. Work is ongoing to improve the representation of soil moisture
868 stress in JULES. Harper *et al.* (2021) investigated alternative parameterisations for β and found that increasing
869 modelled soil depth and therefore plant access to deep soil moisture improved the simulation of soil moisture
870 stress at eddy covariance flux tower sites. In addition, using soil matric potential instead of volumetric water
871 content in the β function allowed for PFT specific parameterisation of soil moisture stress responses to further

Formatted: Font: 10 pt

Formatted: Line spacing: 1.5 lines

872 improve modelled fluxes. Vidale et al. (2021) explored combinations of non-linear β function responses applied
873 at different points in the photosynthesis – g_s pathway (i.e. carbon assimilation, g_s , or mesophyll conductance).
874 They found that treatments allowing β to act on vegetation fluxes via stomatal and mesophyll routes were able to
875 better capture the spatiotemporal variability in water use efficiency during the growing season. However, in
876 addition to these alternative parameterisations of β , further developments to how the soil-plant hydraulic system
877 is represented in JULES are being made, including an optimality based plant hydraulic transport model recently
878 implemented in JULES (Eller et al., 2020).

879 Whilst the development of multi-layer canopy radiation models in LSMs has improved the simulation of radiation
880 and energy within vegetation canopies, the interception of light by plants in JULES, like most LSMs, is not well
881 represented despite being critical to predicting the uptake of carbon by plants (Loew et al., 2014). LSMs generally
882 make the simplifying assumption that leaves are randomly arranged in space, instead of being clustered into tree
883 crowns or around branches, leaving gaps in and around the canopy. Shortwave radiation is used by plants to
884 photosynthesise, and canopy structure has a direct impact on the fraction of this radiation absorbed. Therefore
885 canopy architecture plays an important role in the partitioning of incident solar radiation.
886 photosynthesis, transpiration and momentum fluxes (Braghiere et al., 2019). More recently, alternative
887 approaches are being considered to represent the forest light environment in LSMs to account for the structural
888 effects of vegetation on radiation partitioning, ranging from canopy clumping parameterisations (Braghiere et al.,
889 2019; Braghiere et al., 2020; Braghiere et al., 2021) to 3-dimensional models of the canopy light environment
890 (Hogan et al., 2018; Kobayashi et al., 2012), embedded in radiative transfer schemes, although the latter tend to
891 be computationally expensive (Yang et al., 2001). Braghiere et al. (2019) incorporated canopy clumping from
892 satellite data into JULES which resulted in an increase in carbon uptake by photosynthesis. The greatest effect
893 were in the tropics, where the canopy clumping parameterisation allowed more light to reach the lower layers of
894 the canopy where photosynthesis tends to be limited by light availability.

Formatted: Font: 10 pt

Formatted: Font: 10 pt

Formatted: Font: 10 pt

Formatted: Font: 10 pt

Formatted: Font: 10 pt

Formatted: Font: 10 pt

Formatted: Font: 10 pt

Formatted: Font: 10 pt

895

896 5.5 Conclusions

897 Here we introduce new representations of plant physiological processes into the JULES model, building enhanced
898 capability, and allowing stronger links between model and field studies. This work a) introduces updated
899 understanding of plant physiological processes into JULES, b) increases the flexibility of the modelling capacity
900 within JULES by allowing use of two alternative photosynthesis and g_s schemes, in addition to thermal
901 acclimation of photosynthesis, and c) provides new parameters that are entirely based on large observational
902 datasets. Testing and evaluation at site-level and globally show some key improvements are made to the JULES
903 model. Thermal acclimation of photosynthesis coupled with the optimality-based g_s scheme led to improved
904 simulated carbon fluxes across much of the tropics for the present-day. With about 40% of the world's vegetation
905 carbon residing in tropical forests, they play a crucial role in regulating both regional and global climate through
906 water and carbon cycle dynamics (Erb et al., 2018; Pan et al., 2011). Therefore, accurate representation of tropical
907 carbon fluxes within LSMs is important. Thermal acclimation and the optimality-based g_s scheme also improved
908 simulated carbon fluxes in the high northern latitude forests in the northern hemisphere summer, and the same
909 model configuration also improved simulated water fluxes across much of this region in the same season. The

910 optimality-based Medlyn g_s scheme reduced the LE flux substantially across the northern boreal forests in JJA.
911 This change reflects a more conservative water-use strategy for the needleleaf evergreen tree PFT that dominates
912 in this region as suggested by the global synthesis of experimental data from Lin et al. (2015). The current JULES
913 Jacobs scheme parameterisation does not accurately capture the water-use strategy of this PFT. Our future climate
914 experiment highlights the impact of thermal acclimation on simulating carbon cycle dynamics and energy fluxes
915 in response to long-term warming. The potential impact of this altered stomatal behaviour on land-atmosphere
916 feedbacks via changes in surface energy fluxes will be examined in future coupled simulations.

917

918 **Code/Data availability**

919 JULES-vn5.6 was used for all simulations. The JULES model code ~~and suites used to run the model are~~ available
920 from the Met Office Science Repository Service (MOSRS): ~~<https://code.metoffice.gov.uk/>~~. Registration is
921 required and code is freely available ~~to anyone for non-commercial use (see here for details of licensing~~
922 ~~<https://jules.jchmr.org/content/code>) subject to completion of a software license. Visit the JULES website~~
923 ~~(<https://jules.jchmr.org/content/getting-started>) to register for a MOSRS account. Documentation for the JULES~~
924 ~~model can be found here: <https://jules-lsm.github.io/vn5.6/>~~. The results presented in this paper were obtained by
925 running JULES from the following branch:

926 ~~https://code.metoffice.gov.uk/svn/jules/main/branches/dev/douglasclark/vn5.6_acclimation~~
927 ~~https://code.metoffice.gov.uk/trac/jules/browser/main/branches/dev/douglasclark/vn5.6_acclimation@16578~~.

928 This ~~is~~ was a development branch of JULES-vn5.6 to include thermal acclimation of photosynthesis as described
929 in this paper. ~~This branch can be accessed and downloaded from the Met Office Science Repository Service once~~
930 ~~the user has registered for an account, as outlined above. All developments described in this paper however~~
931 ~~(including thermal acclimation of photosynthesis) are now available in the official released version of JULES-~~
932 ~~vn5.7 and as such can be downloaded directly from the JULES trunk. Documentation for the JULES model is~~
933 ~~located ~~can be found here: <https://jules-lsm.github.io/vn5.6/>~~, Output data from the model simulations, and R scripts~~
934 ~~to produce the plots in the paper are provided at (<https://doi.org/10.5281/zenodo.5825540>). Site-level simulations~~
935 ~~used the rose suite u-br064 (<https://code.metoffice.gov.uk/trac/roses-u/browser/b/r/0/6/4/> at revision 146216) ~~u-~~~~
936 ~~a1752 which is a copy of the u-a1752 JULES suite for FLUXNET 2015 and LBA sites described here~~
937 ~~(<https://code.metoffice.gov.uk/trac/jules/wiki/FluxnetandLbaSites>, and downloaded from here ;~~
938 ~~<https://code.metoffice.gov.uk/trac/roses-u/browser/a/1/7/5/2/> at revision 145397). The global simulations used~~
939 JULES rose suite u-bq898 (<https://code.metoffice.gov.uk/trac/roses-u/browser/b/q/8/9/8/> at revision 181188)
940 which uses the Global Land configuration 7.1 (Wiltshire et al., 2020). ~~Suites can be downloaded from MOSRS~~
941 ~~once the user has registered for an account.~~

942

943 **Competing Interests**

944 The authors declare no competing interests.

945 **Author Contributions**

946 RIO performed simulations and analysis and wrote the first version of the manuscript. DBC, LMM and RIO
947 developed the model. PLV, PCM and MT provided data for the future climate runs, help with developing the

948 JULES suites, and general expertise. CH assisted with analysis. SF and SS provided ancillary data for forcing the
949 model. LMM, CMT, CH, PLV, BEM, PCM and MT contributed to editing the manuscript. All authors contributed
950 to discussions throughout to develop the work.

951
952
953

Acknowledgements

954 This work and its contributors (RJO, LMM, CH, CMT, PLV, PCM, MT and SF) were supported by the UK-China
955 Research & Innovation Partnership Fund through the Met Office Climate Science for Service Partnership (CSSP)
956 China as part of the Newton Fund. R.J.O. acknowledges support from the Natural Environment Research Council,
957 grant NEC05816 LTS-M-UKESM. This work used eddy covariance data acquired and shared by the FLUXNET
958 community, including these networks: AmeriFlux, AfriFlux, AsiaFlux, CarboAfrica, CarboEuropeIP, CarboItaly,
959 CarboMont, ChinaFlux, Fluxnet-Canada, GreenGrass, ICOS, KoFlux, LBA, NECC, OzFlux-TERN, TCOS-
960 Siberia and USCCC. The ERA-Interim reanalysis data are provided by ECMWF and processed by LSCE. The
961 FLUXNET eddy covariance data processing and harmonization was carried out by the European Fluxes Database
962 Cluster, AmeriFlux Management Project, and Fluxdata project of FLUXNET, with the support of CDIAC and
963 ICOS Ecosystem Thematic Center, and the OzFlux, ChinaFlux and AsiaFlux offices.

964

965

966

967

References

968
969

970 Atkin, O. K., Evans, J. R., and Siebke, K.: Relationship between the inhibition of leaf respiration by light and
971 enhancement of leaf dark respiration following light treatment, *Functional Plant Biology*, 25, 437-443,
972 10.1071/PP97159, 1998.

973
974 Atkin, O. K., Scheurwater, I., and Pons, T. L.: High thermal acclimation potential of both photosynthesis and
975 respiration in two lowland *Plantago* species in contrast to an alpine congeneric, *Global Change Biology*, 12,
976 500-515, 10.1111/j.1365-2486.2006.01114.x, 2006.

977
978 Atkin, O. K., Evans, J. R., Ball, M. C., Lambers, H., and Pons, T. L.: Leaf Respiration of Snow Gum in the
979 Light and Dark. Interactions between Temperature and Irradiance1, *Plant Physiology*, 122, 915-924,
980 10.1104/pp.122.3.915, 2000.

981
982 Ball, M. C., Woodrow, I. E., and Berry, J. A.: A model predicting stomatal conductance and its contribution to
983 the control of photosynthesis under different environmental conditions. , In *Progress in Photosynthesis Research*
984 (ed J. Biggins). Martinus Nijhoff Publishers, Dordrecht, Netherlands., 221-224, 1987.

985
986 Benomar, L., Lamhamedi, M. S., Pepin, S., Rainville, A., Lambert, M.-C., Margolis, H. A., Bousquet, J., and
987 Beaulieu, J.: Thermal acclimation of photosynthesis and respiration of southern and northern white spruce seed
988 sources tested along a regional climatic gradient indicates limited potential to cope with temperature warming,
989 *Annals of Botany*, 121, 443-457, 10.1093/aob/mcx174, 2017.

990
991 Bernacchi, C. J., Singsaas, E. L., Pimentel, C., Portis Jr, A. R., and Long, S. P.: Improved temperature response
992 functions for models of Rubisco-limited photosynthesis, *Plant, Cell & Environment*, 24, 253-259,
993 10.1111/j.1365-3040.2001.00668.x, 2001.

994
995 Best, M. J., Pryor, M., Clark, D. B., Rooney, G. G., Essery, R. L. H., Ménard, C. B., Edwards, J. M., Hendry, M.
996 A., Porson, A., Gedney, N., Mercado, L. M., Sitch, S., Blyth, E., Boucher, O., Cox, P. M., Grimmond, C. S. B.,
997 and Harding, R. J.: The Joint UK Land Environment Simulator (JULES), model description – Part 1: Energy
998 and water fluxes, *Geosci. Model Dev.*, 4, 677-699, 10.5194/gmd-4-677-2011, 2011.

1000
1001 Betts, R. A., Boucher, O., Collins, M., Cox, P. M., Falloon, P. D., Gedney, N., Hemming, D. L., Huntingford,
1002 C., Jones, C. D., Sexton, D. M. H., and Webb, M. J.: Projected increase in continental runoff due to plant
1003 responses to increasing carbon dioxide, *Nature*, 448, 1037-1041, 10.1038/nature06045, 2007.

1004
1005 Blyth, E., Clark, D. B., Ellis, R., Huntingford, C., Los, S., Pryor, M., Best, M., and Sitch, S.: A comprehensive
1006 set of benchmark tests for a land surface model of simultaneous fluxes of water and carbon at both the global
1007 and seasonal scale, *Geosci. Model Dev.*, 4, 255-269, 10.5194/gmd-4-255-2011, 2011.

1008
1009 Booth, B. B. B., Jones, C. D., Collins, M., Totterdell, I. J., Cox, P. M., Sitch, S., Huntingford, C., Betts, R. A.,
1010 Harris, G. R., and Lloyd, J.: High sensitivity of future global warming to land carbon cycle processes,
1011 *Environmental Research Letters*, 7, 024002, 10.1088/1748-9326/7/2/024002, 2012.

1012
1013 Braghieri, R. K., Quaife, T., Black, E., He, L., and Chen, J.: Underestimation of global photosynthesis in Earth
1014 system models due to representation of vegetation structure, *Global Biogeochemical Cycles*, 33, 1358-1369,
1015 2019.

1016
1017 Braghieri, R. K., Quaife, T., Black, E., Ryu, Y., Chen, Q., De Kauwe, M. G., and Baldocchi, D.: Influence of
1018 sun zenith angle on canopy clumping and the resulting impacts on photosynthesis, *Agricultural and Forest
1019 Meteorology*, 291, 108065, 10.1016/j.agrformet.2020.108065, 2020.

1020
1021 Braghieri, R. K., Wang, Y., Doughty, R., Sousa, D., Magney, T., Widlowski, J.-L., Longo, M., Bloom, A. A.,
1022 Worden, J., Gentine, P., and Frankenberg, C.: Accounting for canopy structure improves hyperspectral radiative
1023 transfer and sun-induced chlorophyll fluorescence representations in a new generation Earth System model,
1024 *Remote Sensing of Environment*, 261, 112497, 10.1016/j.rse.2021.112497, 2021.

1025
1026 Carter, K. R., Wood, T. E., Reed, S. C., Butts, K. M., and Cavaleri, M. A.: Experimental warming across a
1027 tropical forest canopy height gradient reveals minimal photosynthetic and respiratory acclimation, *Plant, Cell &
1028 Environment*, 44, 2879-2897, 10.1111/pce.14134, 2021.

1029
1030 Carter, K. R., Wood, T. E., Reed, S. C., Schwartz, E. C., Reinsel, M. B., Yang, X., and Cavaleri, M. A.:
1031 Photosynthetic and Respiratory Acclimation of Understory Shrubs in Response to in situ Experimental
1032 Warming of a Wet Tropical Forest, *Frontiers in Forests and Global Change*, 3, 10.3389/ffgc.2020.576320, 2020.

1033
1034 Chen, M. I. N. and Zhuang, Q.: Modelling temperature acclimation effects on the carbon dynamics of forest
1035 ecosystems in the conterminous United States, *Tellus B: Chemical and Physical Meteorology*, 65, 19156,
1036 10.3402/tellusb.v65i0.19156, 2013.

1037
1038 Clark, D. B., Mercado, L. M., Sitch, S., Jones, C. D., Gedney, N., Best, M. J., Pryor, M., Rooney, G. G., Essery,
1039 R. L. H., Blyth, E., Boucher, O., Harding, R. J., Huntingford, C., and Cox, P. M.: The Joint UK Land
1040 Environment Simulator (JULES), model description – Part 2: Carbon fluxes and vegetation dynamics, *Geosci.
1041 Model Dev.*, 4, 701-722, 10.5194/gmd-4-701-2011, 2011.

1042
1043 Collatz, G., Ribas-Carbo, M., and Berry, J.: Coupled Photosynthesis-Stomatal Conductance Model for Leaves
1044 of C₄ Plants, *Functional Plant Biology*, 19, 519-538, 10.1071/PP9920519, 1992.

1045
1046 Collatz, G. J., Ball, J. T., Grivet, C., and Berry, J. A.: Physiological and environmental regulation of stomatal
1047 conductance, photosynthesis and transpiration: a model that includes a laminar boundary layer, *Agricultural and
1048 Forest Meteorology*, 54, 107-136, 10.1016/0168-1923(91)90002-8, 1991.

1049 Cox, P. M., Huntingford, C., and Harding, R. J.: A canopy conductance and photosynthesis model for use in a
1050 GCM land surface scheme, *Journal of Hydrology*, 212-213, 79-94, 10.1016/S0022-1694(98)00203-0, 1998.
1051

1052 Croft, H., Chen, J. M., Luo, X., Bartlett, P., Chen, B., and Staebler, R. M.: Leaf chlorophyll content as a proxy
1053 for leaf photosynthetic capacity, *Global Change Biology*, 23, 3513-3524, 10.1111/gcb.13599, 2017.
1054

1055 Cruz, F. T., Pitman, A. J., and Wang, Y. P.: Can the stomatal response to higher atmospheric carbon dioxide
1056 explain the unusual temperatures during the 2002 Murray-Darling Basin drought?, *Journal of Geophysical
1057 Research: Atmospheres*, 115, 10.1029/2009JD012767, 2010.
1058

1059 Cunningham, S. C. and Read, J.: Do temperate rainforest trees have a greater ability to acclimate to changing
1060 temperatures than tropical rainforest trees?, *New Phytologist*, 157, 55-64, 10.1046/j.1469-8137.2003.00652.x,
1061 2003.
1062

1063 Damour, G., Simonneau, T., Cochard, H., and Urban, L.: An overview of models of stomatal conductance at the
1064 leaf level, *Plant, Cell & Environment*, 33, 1419-1438, 10.1111/j.1365-3040.2010.02181.x, 2010.
1065

1066 de Arellano, J. V.-G., van Heerwaarden, C. C., and Lelieveld, J.: Modelled suppression of boundary-layer
1067 clouds by plants in a CO₂-rich atmosphere, *Nature Geoscience*, 5, 701-704, 10.1038/ngeo1554, 2012.
1068

1069 De Kauwe, M. G., Kala, J., Lin, Y. S., Pitman, A. J., Medlyn, B. E., Duursma, R. A., Abramowitz, G., Wang, Y.
1070 P., and Miralles, D. G.: A test of an optimal stomatal conductance scheme within the CABLE land surface
1071 model, *Geosci. Model Dev.*, 8, 431-452, 10.5194/gmd-8-431-2015, 2015.
1072

1073 De Kauwe, M. G., Medlyn, B. E., Zaehle, S., Walker, A. P., Dietze, M. C., Hickler, T., Jain, A. K., Luo, Y.,
1074 Parton, W. J., Prentice, I. C., Smith, B., Thornton, P. E., Wang, S., Wang, Y.-P., Wårlind, D., Weng, E., Crous,
1075 K. Y., Ellsworth, D. S., Hanson, P. J., Seok Kim, H.-., Warren, J. M., Oren, R., and Norby, R. J.: Forest water
1076 use and water use efficiency at elevated CO₂: a model-data intercomparison at two contrasting temperate forest
1077 FACE sites, *Global Change Biology*, 19, 1759-1779, 10.1111/gcb.12164, 2013.
1078

1079 Doughty, C. E. and Goulden, M. L.: Are tropical forests near a high temperature threshold?, *Journal of
1080 Geophysical Research: Biogeosciences*, 113, 10.1029/2007JG000632, 2008.
1081

1082 Drake, J. E., Aspinwall, M. J., Pfautsch, S., Rymer, P. D., Reich, P. B., Smith, R. A., Crous, K. Y., Tissue, D.
1083 T., Ghannoum, O., and Tjoelker, M. G.: The capacity to cope with climate warming declines from temperate to
1084 tropical latitudes in two widely distributed Eucalyptus species, *Global Change Biology*, 21, 459-472,
1085 10.1111/gcb.12729, 2015.
1086

1087 Dusenge, M. E., Madhavji, S., and Way, D. A.: Contrasting acclimation responses to elevated CO₂ and warming
1088 between an evergreen and a deciduous boreal conifer, *Global Change Biology*, 26, 3639-3657,
1089 10.1111/gcb.15084, 2020.
1090

1091 Dusenge, M. E., Witemann, M., Mujawamariya, M., Ntawuhiganayo, E. B., Zibera, E., Ntirugurirwa, B., Way,
1092 D. A., Nsabimana, D., Uddling, J., and Wallin, G.: Limited thermal acclimation of photosynthesis in tropical
1093 montane tree species, *Global Change Biology*, 27, 4860-4878, 10.1111/gcb.15790, 2021.
1094

1095 Eller, C. B., Rowland, L., Mencuccini, M., Rosas, T., Williams, K., Harper, A., Medlyn, B. E., Wagner, Y.,
1096 Klein, T., Teodoro, G. S., Oliveira, R. S., Matos, I. S., Rosado, B. H. P., Fuchs, K., Wohlfahrt, G., Montagnani,
1097 L., Meir, P., Sitch, S., and Cox, P. M.: Stomatal optimization based on xylem hydraulics (SOX) improves land
1098 surface model simulation of vegetation responses to climate, *New Phytologist*, 226, 1622-1637,
1099 10.1111/nph.16419, 2020.
1100

1101 Erb, K.-H., Kastner, T., Plutzer, C., Bais, A. L. S., Carvalhais, N., Fetzel, T., Gingrich, S., Haberl, H., Lauk, C.,
1102 Niedertscheider, M., Pongratz, J., Thurner, M., and Luyssaert, S.: Unexpectedly large impact of forest
1103 management and grazing on global vegetation biomass, *Nature*, 553, 73-76, 10.1038/nature25138, 2018.
1104

1105 Eyring, V., Bony, S., Meehl, G. A., Senior, C. A., Stevens, B., Stouffer, R. J., and Taylor, K. E.: Overview of
1106 the Coupled Model Intercomparison Project Phase 6 (CMIP6) experimental design and organization, *Geosci.
1107 Model Dev.*, 9, 1937-1958, 10.5194/gmd-9-1937-2016, 2016.
1108

1109 Farquhar, G. D., von Caemmerer, S., and Berry, J. A.: A biochemical model of photosynthetic CO₂ assimilation
1110 in leaves of C₃ species, *Planta*, 149, 78-90, 10.1007/BF00386231, 1980.
1111

1112 Franks, P. J., Berry, J. A., Lombardozi, D. L., and Bonan, G. B.: Stomatal Function across Temporal and
1113 Spatial Scales: Deep-Time Trends, Land-Atmosphere Coupling and Global Models, *Plant Physiology*, 174, 583-
1114 602, 10.1104/pp.17.00287, 2017.
1115

1116 Franks, P. J., Bonan, G. B., Berry, J. A., Lombardozi, D. L., Holbrook, N. M., Herold, N., and Oleson, K. W.:
1117 Comparing optimal and empirical stomatal conductance models for application in Earth system models, *Global
1118 Change Biology*, 24, 5708-5723, 10.1111/gcb.14445, 2018.
1119

1120 Friedlingstein, P., Meinshausen, M., Arora, V. K., Jones, C. D., Anav, A., Liddicoat, S. K., and Knutti, R.:
1121 Uncertainties in CMIP5 Climate Projections due to Carbon Cycle Feedbacks, *Journal of Climate*, 27, 511-526,
1122 10.1175/jcli-d-12-00579.1, 2014.
1123

1124 Friedlingstein, P., O'Sullivan, M., Jones, M. W., Andrew, R. M., Hauck, J., Olsen, A., Peters, G. P., Peters, W.,
1125 Pongratz, J., Sitch, S., Le Quéré, C., Canadell, J. G., Ciais, P., Jackson, R. B., Alin, S., Aragão, L. E. O. C.,
1126 Arneeth, A., Arora, V., Bates, N. R., Becker, M., Benoit-Cattin, A., Bittig, H. C., Bopp, L., Bultan, S., Chandra,
1127 N., Chevallier, F., Chini, L. P., Evans, W., Florentie, L., Forster, P. M., Gasser, T., Gehlen, M., Gilfillan, D.,
1128 Gkrizalis, T., Gregor, L., Gruber, N., Harris, I., Hartung, K., Haverd, V., Houghton, R. A., Ilyina, T., Jain, A.
1129 K., Joetzjer, E., Kadono, K., Kato, E., Kitidis, V., Korsbakken, J. I., Landschützer, P., Lefèvre, N., Lenton, A.,
1130 Lienert, S., Liu, Z., Lombardozi, D., Marland, G., Metzl, N., Munro, D. R., Nabel, J. E. M. S., Nakaoka, S. I.,
1131 Niwa, Y., O'Brien, K., Ono, T., Palmer, P. I., Pierrot, D., Poulter, B., Resplandy, L., Robertson, E., Rödenbeck,
1132 C., Schwinger, J., Séférian, R., Skjelvan, I., Smith, A. J. P., Sutton, A. J., Tanhua, T., Tans, P. P., Tian, H.,
1133 Tilbrook, B., van der Werf, G., Vuichard, N., Walker, A. P., Wanninkhof, R., Watson, A. J., Willis, D.,
1134 Wiltshire, A. J., Yuan, W., Yue, X., and Zaehle, S.: Global Carbon Budget 2020, *Earth Syst. Sci. Data*, 12,
1135 3269-3340, 10.5194/essd-12-3269-2020, 2020.
1136

1137 Gedney, N., Cox, P. M., Betts, R. A., Boucher, O., Huntingford, C., and Stott, P. A.: Detection of a direct
1138 carbon dioxide effect in continental river runoff records, *Nature*, 439, 835-838, 10.1038/nature04504, 2006.
1139

1140 Guha, A., Han, J., Cummings, C., McLennan, D. A., and Warren, J. M.: Differential ecophysiological responses
1141 and resilience to heat wave events in four co-occurring temperate tree species, *Environmental Research Letters*,
1142 13, 065008, 10.1088/1748-9326/aabcd8, 2018.
1143

1144 Gunderson, C. A., Norby, R. J., and Wullschlegel, S. D.: Acclimation of photosynthesis and respiration to
1145 simulated climatic warming in northern and southern populations of *Acer saccharum*: laboratory and field
1146 evidence, *Tree Physiology*, 20, 87-96, 10.1093/treephys/20.2.87, 2000.
1147

1148 Gunderson, C. A., O'Hara, K. H., Campion, C. M., Walker, A. V., and Edwards, N. T.: Thermal plasticity of
1149 photosynthesis: the role of acclimation in forest responses to a warming climate, *Global Change Biology*, 16,
1150 2272-2286, 10.1111/j.1365-2486.2009.02090.x, 2010.
1151

1152 Haarsma, R. J., Roberts, M. J., Vidale, P. L., Senior, C. A., Bellucci, A., Bao, Q., Chang, P., Corti, S., Fučkar,
1153 N. S., Guemas, V., von Hardenberg, J., Hazeleger, W., Kodama, C., Koenigk, T., Leung, L. R., Lu, J., Luo, J. J.,
1154 Mao, J., Mizielinski, M. S., Mizuta, R., Nobre, P., Satoh, M., Scoccimarro, E., Semmler, T., Small, J., and von
1155 Storch, J. S.: High Resolution Model Intercomparison Project (HighResMIP v1.0) for CMIP6, *Geosci. Model
1156 Dev.*, 9, 4185-4208, 10.5194/gmd-9-4185-2016, 2016.
1157

1158 Harper, A. B., Cox, P. M., Friedlingstein, P., Wiltshire, A. J., Jones, C. D., Sitch, S., Mercado, L. M.,
1159 Groenendijk, M., Robertson, E., Kattge, J., Bönisch, G., Atkin, O. K., Bahn, M., Cornelissen, J., Niinemets, Ü.,
1160 Onipchenko, V., Peñuelas, J., Poorter, L., Reich, P. B., Soudzilovskaia, N. A., and Bodegom, P. V.: Improved
1161 representation of plant functional types and physiology in the Joint UK Land Environment Simulator (JULES
1162 v4.2) using plant trait information, *Geosci. Model Dev.*, 9, 2415-2440, 10.5194/gmd-9-2415-2016, 2016.
1163

1164 Harper, A. B., Williams, K. E., McGuire, P. C., Duran Rojas, M. C., Hemming, D., Verhoef, A., Huntingford,
1165 C., Rowland, L., Marthews, T., Breder Eller, C., Mathison, C., Nobrega, R. L. B., Gedney, N., Vidale, P. L.,
1166 Otu-Larbi, F., Pandey, D., Garrigues, S., Wright, A., Slevin, D., De Kauwe, M. G., Blyth, E., Ardö, J., Black,
1167 A., Bonal, D., Buchmann, N., Burban, B., Fuchs, K., de Grandcourt, A., Mammarella, I., Merbold, L.,
1168 Montagnani, L., Nouvellon, Y., Restrepo-Coupe, N., and Wohlfahrt, G.: Improvement of modeling plant

1169 responses to low soil moisture in JULESv4.9 and evaluation against flux tower measurements, *Geosci. Model*
1170 *Dev.*, 14, 3269-3294, 10.5194/gmd-14-3269-2021, 2021.

1171

1172 Hengl, T., de Jesus, J. M., MacMillan, R. A., Batjes, N. H., Heuvelink, G. B. M., Ribeiro, E., Samuel-Rosa, A.,
1173 Kempen, B., Leenaars, J. G. B., Walsh, M. G., and Gonzalez, M. R.: SoilGrids1km — Global Soil Information
1174 Based on Automated Mapping, *PLOS ONE*, 9, e105992, 10.1371/journal.pone.0105992, 2014.

1175

1176 Hernández, G. G., Winter, K., and Slot, M.: Similar temperature dependence of photosynthetic parameters in
1177 sun and shade leaves of three tropical tree species, *Tree Physiology*, 40, 637-651, 10.1093/treephys/tpaa015,
1178 2020.

1179

1180 Hikosaka, K., Nabeshima, E., and Hiura, T.: Seasonal changes in the temperature response of photosynthesis in
1181 canopy leaves of *Quercus crispula* in a cool-temperate forest, *Tree Physiology*, 27, 1035-1041,
1182 10.1093/treephys/27.7.1035, 2007.

1183

1184 Hogan, R. J., Quaife, T., and Braghieri, R.: Fast matrix treatment of 3-D radiative transfer in vegetation
1185 canopies: SPARTACUS-Vegetation 1.1, *Geoscientific Model Development*, 11, 339-350, 2018.

1186

1187 Huntingford, C. and Oliver, R. J.: Converging towards a common representation of large-scale photosynthesis,
1188 *Global Change Biology*, 27, 716-718, 10.1111/gcb.15398, 2021.

1189

1190 Huntingford, C., Lowe, J. A., Booth, B. B. B., Jones, C. D., Harris, G. R., Gohar, L. K., and Meir, P.:
1191 Contributions of carbon cycle uncertainty to future climate projection spread, *Tellus B: Chemical and Physical*
1192 *Meteorology*, 61, 355-360, 10.1111/j.1600-0889.2008.00414.x, 2009.

1193

1194 Jacobs, C. M. J.: Direct impact of atmospheric CO₂ enrichment on regional transpiration, *Jacobs, S.I.*, 1994.

1195

1196 Jarvis, P. G., Monteith, J. L., and Weatherley, P. E.: The interpretation of the variations in leaf water potential
1197 and stomatal conductance found in canopies in the field, *Philosophical Transactions of the Royal Society of*
1198 *London. B, Biological Sciences*, 273, 593-610, doi:10.1098/rstb.1976.0035, 1976.

1199

1200 Jasechko, S., Sharp, Z. D., Gibson, J. J., Birks, S. J., Yi, Y., and Fawcett, P. J.: Terrestrial water fluxes
1201 dominated by transpiration, *Nature*, 496, 347-350, 10.1038/nature11983, 2013.

1202

1203 Jogireddy, V. R., Cox, P. M., Huntingford, C., Harding, R. J., and Mercado, L. M.: An improved description of
1204 canopy light interception for use in a GCM land-surface scheme: calibration and testing against carbon fluxes at
1205 a coniferous forest, *Hadley Centre Technical Note 63*, Hadley Centre, Met Office, Exeter, UK, 2006.

1206

1207 Joseph, T., Whitehead, D., and Turnbull, M. H.: Soil water availability influences the temperature response of
1208 photosynthesis and respiration in a grass and a woody shrub, *Functional Plant Biology*, 41, 468-481,
1209 10.1071/FP13237, 2014.

1210

1211 Jung, M., Koirala, S., Weber, U., Ichii, K., Gans, F., Camps-Valls, G., Papale, D., Schwalm, C., Tramontana,
1212 G., and Reichstein, M.: The FLUXCOM ensemble of global land-atmosphere energy fluxes, *Scientific Data*, 6,
1213 74, 10.1038/s41597-019-0076-8, 2019.

1214

1215 Jung, M., Schwalm, C., Migliavacca, M., Walther, S., Camps-Valls, G., Koirala, S., Anthoni, P., Besnard, S.,
1216 Bodesheim, P., Carvalhais, N., Chevallier, F., Gans, F., Goll, D. S., Haverd, V., Köhler, P., Ichii, K., Jain, A. K.,
1217 Liu, J., Lombardozi, D., Nabel, J. E. M. S., Nelson, J. A., O'Sullivan, M., Pallandt, M., Papale, D., Peters, W.,
1218 Pongratz, J., Rödenbeck, C., Sitch, S., Tramontana, G., Walker, A., Weber, U., and Reichstein, M.: Scaling
1219 carbon fluxes from eddy covariance sites to globe: synthesis and evaluation of the FLUXCOM approach,
1220 *Biogeosciences*, 17, 1343-1365, 10.5194/bg-17-1343-2020, 2020.

1221

1222 Kala, J., De Kauwe, M. G., Pitman, A. J., Medlyn, B. E., Wang, Y.-P., Lorenz, R., and Perkins-Kirkpatrick, S.
1223 E.: Impact of the representation of stomatal conductance on model projections of heatwave intensity, *Scientific*
1224 *Reports*, 6, 23418, 10.1038/srep23418, 2016.

1225

1226 Kala, J., De Kauwe, M. G., Pitman, A. J., Lorenz, R., Medlyn, B. E., Wang, Y. P., Lin, Y. S., and Abramowitz,
1227 G.: Implementation of an optimal stomatal conductance scheme in the Australian Community Climate Earth
1228 Systems Simulator (ACCESS1.3b), *Geosci. Model Dev.*, 8, 3877-3889, 10.5194/gmd-8-3877-2015, 2015.

1229
1230 Kattge, J. and Knorr, W.: Temperature acclimation in a biochemical model of photosynthesis: a reanalysis of
1231 data from 36 species, *Plant, Cell & Environment*, 30, 1176-1190, 10.1111/j.1365-3040.2007.01690.x, 2007.
1232
1233 Keenan, T. F., Luo, X., De Kauwe, M. G., Medlyn, B. E., Prentice, I. C., Stocker, B. D., Smith, N. G., Terrer,
1234 C., Wang, H., Zhang, Y., and Zhou, S.: A constraint on historic growth in global photosynthesis due to
1235 increasing CO₂, *Nature*, 600, 253-258, 10.1038/s41586-021-04096-9, 2021.
1236
1237 Kobayashi, H., Baldocchi, D. D., Ryu, Y., Chen, Q., Ma, S., Osuna, J. L., and Ustin, S. L.: Modeling energy and
1238 carbon fluxes in a heterogeneous oak woodland: A three-dimensional approach, *Agricultural and Forest
1239 Meteorology*, 152, 83-100, 2012.
1240
1241 Kooperman, G. J., Chen, Y., Hoffman, F. M., Koven, C. D., Lindsay, K., Pritchard, M. S., Swann, A. L. S., and
1242 Randerson, J. T.: Forest response to rising CO₂ drives zonally asymmetric rainfall change over tropical land,
1243 *Nature Climate Change*, 8, 434-440, 10.1038/s41558-018-0144-7, 2018.
1244
1245 Krinner, G., Viovy, N., de Noblet-Ducoudré, N., Ogée, J., Polcher, J., Friedlingstein, P., Ciais, P., Sitch, S., and
1246 Prentice, I. C.: A dynamic global vegetation model for studies of the coupled atmosphere-biosphere system,
1247 *Global Biogeochemical Cycles*, 19, 10.1029/2003GB002199, 2005.
1248
1249 Kroner, Y. and Way, D. A.: Carbon fluxes acclimate more strongly to elevated growth temperatures than to
1250 elevated CO₂ concentrations in a northern conifer, *Global Change Biology*, 22, 2913-2928, 10.1111/gcb.13215,
1251 2016.
1252
1253 Kumarathunge, D. P., Medlyn, B. E., Drake, J. E., Rogers, A., and Tjoelker, M. G.: No evidence for triose
1254 phosphate limitation of light-saturated leaf photosynthesis under current atmospheric CO₂ concentration, *Plant,
1255 Cell & Environment*, 42, 3241-3252, 10.1111/pce.13639, 2019a.
1256
1257 Kumarathunge, D. P., Medlyn, B. E., Drake, J. E., Tjoelker, M. G., Aspinwall, M. J., Battaglia, M., Cano, F. J.,
1258 Carter, K. R., Cavaleri, M. A., Cernusak, L. A., Chambers, J. Q., Crous, K. Y., De Kauwe, M. G., Dillaway, D.
1259 N., Dreyer, E., Ellsworth, D. S., Ghannoum, O., Han, Q., Hikosaka, K., Jensen, A. M., Kelly, J. W. G., Kruger,
1260 E. L., Mercado, L. M., Onoda, Y., Reich, P. B., Rogers, A., Slot, M., Smith, N. G., Tarvainen, L., Tissue, D. T.,
1261 Togashi, H. F., Tribuzy, E. S., Uddling, J., Vårhammar, A., Wallin, G., Warren, J. M., and Way, D. A.:
1262 Acclimation and adaptation components of the temperature dependence of plant photosynthesis at the global
1263 scale, *New Phytologist*, 222, 768-784, 10.1111/nph.15668, 2019b.
1264
1265 Kurepin, L. V., Stangl, Z. R., Ivanov, A. G., Bui, V., Mema, M., Hüner, N. P. A., Öquist, G., Way, D., and
1266 Hurry, V.: Contrasting acclimation abilities of two dominant boreal conifers to elevated CO₂ and temperature,
1267 *Plant, Cell & Environment*, 41, 1331-1345, 10.1111/pce.13158, 2018.
1268
1269 Leuning, R.: A critical appraisal of a combined stomatal-photosynthesis model for C₃ plants, *Plant, Cell &
1270 Environment*, 18, 339-355, 10.1111/j.1365-3040.1995.tb00370.x, 1995.
1271
1272 Lin, Y.-S., Medlyn, B. E., Duursma, R. A., Prentice, I. C., Wang, H., Baig, S., Eamus, D., de Dios, Victor R.,
1273 Mitchell, P., Ellsworth, D. S., de Beeck, M. O., Wallin, G., Uddling, J., Tarvainen, L., Linderson, M.-L.,
1274 Cernusak, L. A., Nippert, J. B., Ocheltree, T. W., Tissue, D. T., Martin-StPaul, N. K., Rogers, A., Warren, J. M.,
1275 De Angelis, P., Hikosaka, K., Han, Q., Onoda, Y., Gimeno, T. E., Barton, C. V. M., Bennie, J., Bonal, D., Bosc,
1276 A., Löw, M., Macinins-Ng, C., Rey, A., Rowland, L., Setterfield, S. A., Tausz-Posch, S., Zaragoza-Castells, J.,
1277 Broadmeadow, M. S. J., Drake, J. E., Freeman, M., Ghannoum, O., Hutley, Lindsay B., Kelly, J. W., Kikuzawa,
1278 K., Kolar, P., Koyama, K., Limousin, J.-M., Meir, P., Lola da Costa, A. C., Mikkelsen, T. N., Salinas, N., Sun,
1279 W., and Wingate, L.: Optimal stomatal behaviour around the world, *Nature Climate Change*, 5, 459-464,
1280 10.1038/nclimate2550, 2015.
1281
1282 Liu, H., Randerson, J. T., Lindfors, J., Massman, W. J., and Foken, T.: Consequences of Incomplete Surface
1283 Energy Balance Closure for CO₂ Fluxes from Open-Path CO₂/H₂O Infrared Gas Analysers, *Boundary-Layer
1284 Meteorology*, 120, 65-85, 10.1007/s10546-005-9047-z, 2006.
1285
1286 Loew, A., Van Bodegom, P., Widłowski, J.-L., Otto, J., Quaife, T., Pinty, B., and Raddatz, T.: Do we (need to)
1287 care about canopy radiation schemes in DGVMs? Caveats and potential impacts, *Biogeosciences*, 11, 1873-
1288 1897, 2014.

1289
1290 Lombardozzi, D. L., Bonan, G. B., Smith, N. G., Dukes, J. S., and Fisher, R. A.: Temperature acclimation of
1291 photosynthesis and respiration: A key uncertainty in the carbon cycle-climate feedback, *Geophysical Research*
1292 *Letters*, 42, 8624-8631, 10.1002/2015GL065934, 2015.

1293
1294 Mau, A. C., Reed, S. C., Wood, T. E., and Cavaleri, M. A.: Temperate and Tropical Forest Canopies are
1295 Already Functioning beyond Their Thermal Thresholds for Photosynthesis, *Forests*, 9, 47, 2018.

1296
1297 Medlyn, B. E., Loustau, D., and Delzon, S.: Temperature response of parameters of a biochemically based
1298 model of photosynthesis. I. Seasonal changes in mature maritime pine (*Pinus pinaster* Ait.), *Plant, Cell &*
1299 *Environment*, 25, 1155-1165, 10.1046/j.1365-3040.2002.00890.x, 2002.

1300
1301 Medlyn, B. E., Duursma, R. A., Eamus, D., Ellsworth, D. S., Prentice, I. C., Barton, C. V. M., Crous, K. Y., de
1302 Angelis, P., Freeman, M., and Wingate, L.: Reconciling the optimal and empirical approaches to modelling
1303 stomatal conductance, *Global Change Biology*, 17, 2134-2144, 10.1111/j.1365-2486.2010.02375.x, 2011.

1304
1305 Meir, P., Kruijt, B., Broadmeadow, M., Barbosa, E., Kull, O., Carswell, F., Nobre, A., and Jarvis, P. G.:
1306 Acclimation of photosynthetic capacity to irradiance in tree canopies in relation to leaf nitrogen concentration
1307 and leaf mass per unit area, *Plant, Cell & Environment*, 25, 343-357, 10.1046/j.0016-8025.2001.00811.x, 2002.

1308
1309 Mercado, L. M., Huntingford, C., Gash, J. H. C., Cox, P. M., and Jogireddy, V. R.: Improving the representation
1310 of radiation interception and photosynthesis for climate model applications, *Tellus B*, 59, 553-565,
1311 10.1111/j.1600-0889.2007.00256.x, 2007.

1312
1313 Mercado, L. M., Bellouin, N., Sitch, S., Boucher, O., Huntingford, C., Wild, M., and Cox, P. M.: Impact of
1314 changes in diffuse radiation on the global land carbon sink, *Nature*, 458, 1014-1017, 10.1038/nature07949,
1315 2009.

1316
1317 Mercado, L. M., Medlyn, B. E., Huntingford, C., Oliver, R. J., Clark, D. B., Sitch, S., Zelazowski, P., Kattge, J.,
1318 Harper, A. B., and Cox, P. M.: Large sensitivity in land carbon storage due to geographical and temporal
1319 variation in the thermal response of photosynthetic capacity, *New Phytologist*, 218, 1462-1477,
1320 10.1111/nph.15100, 2018.

1321
1322 Miller, B. D., Carter, K. R., Reed, S. C., Wood, T. E., and Cavaleri, M. A.: Only sun-lit leaves of the uppermost
1323 canopy exceed both air temperature and photosynthetic thermal optima in a wet tropical forest, *Agricultural and*
1324 *Forest Meteorology*, 301-302, 108347, 10.1016/j.agrformet.2021.108347, 2021.

1325
1326 Oliver, R. J., Mercado, L. M., Sitch, S., Simpson, D., Medlyn, B. E., Lin, Y. S., and Folberth, G. A.: Large but
1327 decreasing effect of ozone on the European carbon sink, *Biogeosciences*, 15, 4245-4269, 10.5194/bg-15-4245-
1328 2018, 2018.

1329
1330 Pan, Y., Birdsey, R. A., Fang, J., Houghton, R., Kauppi, P. E., Kurz, W. A., Phillips, O. L., Shvidenko, A.,
1331 Lewis, S. L., Canadell, J. G., Ciais, P., Jackson, R. B., Pacala, S. W., McGuire, A. D., Piao, S., Rautiainen, A.,
1332 Sitch, S., and Hayes, D.: A Large and Persistent Carbon Sink in the World's Forests, *Science*, 333, 988-993,
1333 10.1126/science.1201609, 2011.

1334
1335 Pau, S., Detto, M., Kim, Y., and Still, C. J.: Tropical forest temperature thresholds for gross primary
1336 productivity, *Ecosphere*, 9, e02311, 10.1002/ecs2.2311, 2018.

1337
1338 Poulter, B., MacBean, N., Hartley, A., Khlystova, I., Arino, O., Betts, R., Bontemps, S., Boettcher, M.,
1339 Brockmann, C., Defourny, P., Hagemann, S., Herold, M., Kirches, G., Lamarche, C., Lederer, D., Ottlé, C.,
1340 Peters, M., and Peylin, P.: Plant functional type classification for earth system models: results from the
1341 European Space Agency's Land Cover Climate Change Initiative, *Geosci. Model Dev.*, 8, 2315-2328,
1342 10.5194/gmd-8-2315-2015, 2015.

1343
1344 Reich, P. B., Sendall, K. M., Stefanski, A., Rich, R. L., Hobbie, S. E., and Montgomery, R. A.: Effects of
1345 climate warming on photosynthesis in boreal tree species depend on soil moisture, *Nature*, 562, 263-267,
1346 10.1038/s41586-018-0582-4, 2018.

1347

1348 Roberts, M. J., Baker, A., Blockley, E. W., Calvert, D., Coward, A., Hewitt, H. T., Jackson, L. C., Kuhlbrodt,
1349 T., Mathiot, P., Roberts, C. D., Schiemann, R., Seddon, J., Vannière, B., and Vidale, P. L.: Description of the
1350 resolution hierarchy of the global coupled HadGEM3-GC3.1 model as used in CMIP6 HighResMIP
1351 experiments, *Geosci. Model Dev.*, 12, 4999-5028, 10.5194/gmd-12-4999-2019, 2019.
1352

1353 Rogers, A., Kumarathunge, D. P., Lombardozi, D. L., Medlyn, B. E., Serbin, S. P., and Walker, A. P.: Triose
1354 phosphate utilization limitation: an unnecessary complexity in terrestrial biosphere model representation of
1355 photosynthesis, *New Phytologist*, 230, 17-22, 10.1111/nph.17092, 2021.
1356

1357 Rogers, A., Medlyn, B. E., Dukes, J. S., Bonan, G., von Caemmerer, S., Dietze, M. C., Kattge, J., Leakey, A. D.
1358 B., Mercado, L. M., Niinemets, Ü., Prentice, I. C., Serbin, S. P., Sitch, S., Way, D. A., and Zaehle, S.: A
1359 roadmap for improving the representation of photosynthesis in Earth system models, *New Phytologist*, 213, 22-
1360 42, 10.1111/nph.14283, 2017.
1361

1362 Schlesinger, W. H. and Jasechko, S.: Transpiration in the global water cycle, *Agricultural and Forest
1363 Meteorology*, 189-190, 115-117, 10.1016/j.agrformet.2014.01.011, 2014.
1364

1365 Sellar, A. A., Jones, C. G., Mulcahy, J. P., Tang, Y., Yool, A., Wiltshire, A., O'Connor, F. M., Stringer, M., Hill,
1366 R., Palmieri, J., Woodward, S., de Mora, L., Kuhlbrodt, T., Rumbold, S. T., Kelley, D. I., Ellis, R., Johnson, C.
1367 E., Walton, J., Abraham, N. L., Andrews, M. B., Andrews, T., Archibald, A. T., Berthou, S., Burke, E.,
1368 Blockley, E., Carslaw, K., Dalvi, M., Edwards, J., Folberth, G. A., Gedney, N., Griffiths, P. T., Harper, A. B.,
1369 Hendry, M. A., Hewitt, A. J., Johnson, B., Jones, A., Jones, C. D., Keeble, J., Liddicoat, S., Morgenstern, O.,
1370 Parker, R. J., Predoi, V., Robertson, E., Siahann, A., Smith, R. S., Swaminathan, R., Woodhouse, M. T., Zeng,
1371 G., and Zerroukat, M.: UKESM1: Description and Evaluation of the U.K. Earth System Model, *Journal of
1372 Advances in Modeling Earth Systems*, 11, 4513-4558, 10.1029/2019MS001739, 2019.
1373

1374 Sendall, K. M., Reich, P. B., Zhao, C., Jihua, H., Wei, X., Stefanski, A., Rice, K., Rich, R. L., and Montgomery,
1375 R. A.: Acclimation of photosynthetic temperature optima of temperate and boreal tree species in response to
1376 experimental forest warming, *Global Change Biology*, 21, 1342-1357, 10.1111/gcb.12781, 2015.
1377

1378 Shabanov, N., Huang, D., Yang, W., Tan, B., Knyazikhin, Y., Myneni, R., Ahl, D., Gower, S., Huete, A.,
1379 Aragao, L., and Shimabukuro, Y.: Analysis and Optimization of the MODIS Leaf Area Index Algorithm
1380 Retrievals Over Broadleaf Forests, *IEEE T. Geosci. Remote*, 43, 1855-1865, doi:10.1109/TGRS.2005.852477,
1381 2005.
1382

1383 Slot, M. and Winter, K.: Photosynthetic acclimation to warming in tropical forest tree seedlings, *Journal of
1384 Experimental Botany*, 68, 2275-2284, 10.1093/jxb/erx071, 2017.
1385

1386 Slot, M., Rifai, S. W., and Winter, K.: Photosynthetic plasticity of a tropical tree species, *Tabebuia rosea*, in
1387 response to elevated temperature and CO₂, *Plant, Cell & Environment*, n/a, 10.1111/pce.14049, 2021.
1388

1389 Smith, N. G. and Dukes, J. S.: Plant respiration and photosynthesis in global-scale models: incorporating
1390 acclimation to temperature and CO₂, *Global Change Biology*, 19, 45-63, 10.1111/j.1365-2486.2012.02797.x,
1391 2013.
1392

1393 Smith, N. G., Malyshev, S. L., Shevliakova, E., Kattge, J., and Dukes, J. S.: Foliar temperature acclimation
1394 reduces simulated carbon sensitivity to climate, *Nature Climate Change*, 6, 407-411, 10.1038/nclimate2878,
1395 2016.
1396

1397 Spafford, L. and MacDougall, A. H.: Validation of terrestrial biogeochemistry in CMIP6 Earth system models: a
1398 review, *Geosci. Model Dev.*, 14, 5863-5889, 10.5194/gmd-14-5863-2021, 2021.
1399

1400 Sullivan, M. J. P., Lewis, S. L., Affum-Baffoe, K., Castilho, C., Costa, F., Sanchez, A. C., Ewango, C. E. N.,
1401 Hubau, W., Marimon, B., Monteagudo-Mendoza, A., Qie, L., Sonké, B., Martinez, R. V., Baker, T. R., Brienien,
1402 R. J. W., Feldpausch, T. R., Galbraith, D., Gloor, M., Malhi, Y., Aiba, S.-I., Alexiades, M. N., Almeida, E. C.,
1403 de Oliveira, E. A., Dávila, E. Á., Loayza, P. A., Andrade, A., Vieira, S. A., Aragão, L. E. O. C., Araujo-
1404 Murakami, A., Arets, E. J. M. M., Arroyo, L., Ashton, P., Aymard C., G., Baccaro, F. B., Banin, L. F., Baraloto,
1405 C., Camargo, P. B., Barlow, J., Barroso, J., Bastin, J.-F., Batterman, S. A., Beeckman, H., Begne, S. K., Bennett,
1406 A. C., Berenguer, E., Berry, N., Blanc, L., Boeckx, P., Bogaert, J., Bonal, D., Bongers, F., Bradford, M.,
1407 Brearley, F. Q., Brncic, T., Brown, F., Burban, B., Camargo, J. L., Castro, W., Céron, C., Ribeiro, S. C.,

1408 Moscoso, V. C., Chave, J., Chezeaux, E., Clark, C. J., de Souza, F. C., Collins, M., Comiskey, J. A., Valverde,
 1409 F. C., Medina, M. C., da Costa, L., Dančák, M., Dargie, G. C., Davies, S., Cardozo, N. D., de Haulleville, T., de
 1410 Medeiros, M. B., del Aguila Pasquel, J., Derroire, G., Di Fiore, A., Doucet, J.-L., Dourdain, A., Droissart, V.,
 1411 Duque, L. F., Ekoungoulou, R., Elias, F., Erwin, T., Esquivel-Muelbert, A., Fauset, S., Ferreira, J., Llampazo,
 1412 G. F., Foli, E., Ford, A., Gilpin, M., Hall, J. S., Hamer, K. C., Hamilton, A. C., Harris, D. J., Hart, T. B., Hédli,
 1413 R., Herault, B., Herrera, R., Higuchi, N., Hladik, A., Coronado, E. H., Huamantupa-Chuquimaco, I., Huasco, W.
 1414 H., Jeffery, K. J., Jimenez-Rojas, E., Kalamandeen, M., Djuikouo, M. N. K., Kearsley, E., Umetsu, R. K., Kho,
 1415 L. K., Killeen, T., Kitayama, K., Klitgaard, B., Koch, A., Labrière, N., Laurance, W., Laurance, S., Leal, M. E.,
 1416 Levesley, A., Lima, A. J. N., Lisingo, J., Lopes, A. P., Lopez-Gonzalez, G., Lovejoy, T., Lovett, J. C., Lowe, R.,
 1417 Magnusson, W. E., Malumbres-Olarte, J., Manzatto, Â. G., Marimon, B. H., Marshall, A. R., Marthews, T., de
 1418 Almeida Reis, S. M., Maycock, C., Melgaço, K., Mendoza, C., Metali, F., Mihindou, V., Milliken, W.,
 1419 Mitchard, E. T. A., Morandi, P. S., Mossman, H. L., Nagy, L., Nascimento, H., Neill, D., Nilus, R., Vargas, P.
 1420 N., Palacios, W., Camacho, N. P., Peacock, J., Pendry, C., Peñuela Mora, M. C., Pickavance, G. C., Pipoly, J.,
 1421 Pitman, N., Playfair, M., Poorter, L., Poulsen, J. R., Poulsen, A. D., Preziosi, R., Prieto, A., Primack, R. B.,
 1422 Ramírez-Angulo, H., Reitsma, J., Réjou-Méchain, M., Correa, Z. R., de Sousa, T. R., Bayona, L. R., Roopsind,
 1423 A., Rudas, A., Rutishauser, E., Abu Salim, K., Salomão, R. P., Schiatti, J., Sheil, D., Silva, R. C., Espejo, J. S.,
 1424 Valeria, C. S., Silveira, M., Simo-Droissart, M., Simon, M. F., Singh, J., Soto Shareva, Y. C., Stahl, C., Stropp,
 1425 J., Sukri, R., Sunderland, T., Svátek, M., Swaine, M. D., Swamy, V., Taedoumg, H., Talbot, J., Taplin, J.,
 1426 Taylor, D., ter Steege, H., Terborgh, J., Thomas, R., Thomas, S. C., Torres-Lezama, A., Umunay, P., Gamarra,
 1427 L. V., van der Heijden, G., van der Hout, P., van der Meer, P., van Nieuwstadt, M., Verbeeck, H., Vernimmen,
 1428 R., Vicentini, A., Vieira, I. C. G., Torre, E. V., Vleminckx, J., Vos, V., Wang, O., White, L. J. T., Willcock, S.,
 1429 Woods, J. T., Wortel, V., Young, K., Zagt, R., Zedler, J., Zuidema, P. A., Zwerts, J. A., and Phillips, O. L.:
 1430 Long-term thermal sensitivity of Earth's tropical forests, *Science*, 368, 869-874, 10.1126/science.aaw7578,
 1431 2020.
 1432
 1433 Tramontana, G., Jung, M., Schwalm, C. R., Ichii, K., Camps-Valls, G., Ráduly, B., Reichstein, M., Arain, M.
 1434 A., Cescatti, A., Kiely, G., Merbold, L., Serrano-Ortiz, P., Sickert, S., Wolf, S., and Papale, D.: Predicting
 1435 carbon dioxide and energy fluxes across global FLUXNET sites with regression algorithms, *Biogeosciences*, 13,
 1436 4291-4313, 10.5194/bg-13-4291-2016, 2016.
 1437
 1438 Vårhammar, A., Wallin, G., McLean, C. M., Dusenge, M. E., Medlyn, B. E., Hasper, T. B., Nsabimana, D., and
 1439 Uddling, J.: Photosynthetic temperature responses of tree species in Rwanda: evidence of pronounced negative
 1440 effects of high temperature in montane rainforest climax species, *New Phytologist*, 206, 1000-1012,
 1441 10.1111/nph.13291, 2015.
 1442
 1443 Verhoef, A. and Egea, G.: Modeling plant transpiration under limited soil water: Comparison of different plant
 1444 and soil hydraulic parameterizations and preliminary implications for their use in land surface models,
 1445 *Agricultural and Forest Meteorology*, 191, 22-32, 10.1016/j.agrformet.2014.02.009, 2014.
 1446
 1447 Vidale, P. L., Egea, G., McGuire, P. C., Todt, M., Peters, W., Müller, O., Balan-Sarajini, B., and Verhoef, A.:
 1448 On the Treatment of Soil Water Stress in GCM Simulations of Vegetation Physiology, *Frontiers in*
 1449 *Environmental Science*, 9, 10.3389/fenvs.2021.689301, 2021.
 1450
 1451 Walker, A. P., Beckerman, A. P., Gu, L., Kattge, J., Cernusak, L. A., Domingues, T. F., Scales, J. C., Wohlfahrt,
 1452 G., Wullschlegel, S. D., and Woodward, F. I.: The relationship of leaf photosynthetic traits – V_{cmax} and J_{max} –
 1453 to leaf nitrogen, leaf phosphorus, and specific leaf area: a meta-analysis and modeling study, *Ecology and*
 1454 *Evolution*, 4, 3218-3235, 10.1002/ece3.1173, 2014.
 1455
 1456 Walker, A. P., Johnson, A. L., Rogers, A., Anderson, J., Bridges, R. A., Fisher, R. A., Lu, D., Ricciuto, D. M.,
 1457 Serbin, S. P., and Ye, M.: Multi-hypothesis comparison of Farquhar and Collatz photosynthesis models reveals
 1458 the unexpected influence of empirical assumptions at leaf and global scales, *Global Change Biology*, 27, 804-
 1459 822, 10.1111/gcb.15366, 2021.
 1460
 1461 Way, D. A. and Sage, R. F.: Elevated growth temperatures reduce the carbon gain of black spruce [*Picea*
 1462 *mariana* (Mill.) B.S.P.], *Global Change Biology*, 14, 624-636, 10.1111/j.1365-2486.2007.01513.x, 2008.
 1463
 1464 Way, D. A. and Yamori, W.: Thermal acclimation of photosynthesis: on the importance of adjusting our
 1465 definitions and accounting for thermal acclimation of respiration, *Photosynthesis Research*, 119, 89-100,
 1466 10.1007/s11120-013-9873-7, 2014.

1467 Way, D. A., Stinziano, J. R., Berghoff, H., and Oren, R.: How well do growing season dynamics of
1468 photosynthetic capacity correlate with leaf biochemistry and climate fluctuations?, *Tree Physiology*, 37, 879-
1469 888, 10.1093/treephys/tpx086, 2017.

1470
1471 Weedon, G. P., Balsamo, G., Bellouin, N., Gomes, S., Best, M. J., and Viterbo, P.: The WFDEI meteorological
1472 forcing data set: WATCH Forcing Data methodology applied to ERA-Interim reanalysis data, *Water Resources*
1473 *Research*, 50, 7505-7514, 10.1002/2014WR015638, 2014.

1474
1475 Williams, K. D., Copsey, D., Blockley, E. W., Bodas-Salcedo, A., Calvert, D., Comer, R., Davis, P., Graham,
1476 T., Hewitt, H. T., Hill, R., Hyder, P., Ineson, S., Johns, T. C., Keen, A. B., Lee, R. W., Megann, A., Milton, S.
1477 F., Rae, J. G. L., Roberts, M. J., Scaife, A. A., Schiemann, R., Storkey, D., Thorpe, L., Watterson, I. G.,
1478 Walters, D. N., West, A., Wood, R. A., Woollings, T., and Xavier, P. K.: The Met Office Global Coupled Model
1479 3.0 and 3.1 (GC3.0 and GC3.1) Configurations, *Journal of Advances in Modeling Earth Systems*, 10, 357-380,
1480 10.1002/2017MS001115, 2018.

1481
1482 Wilson, K. B., Baldocchi, D. D., and Hanson, P. J.: Leaf age affects the seasonal pattern of photosynthetic
1483 capacity and net ecosystem exchange of carbon in a deciduous forest, *Plant, Cell & Environment*, 24, 571-583,
1484 2001.

1485
1486 Wiltshire, A. J., Duran Rojas, M. C., Edwards, J. M., Gedney, N., Harper, A. B., Hartley, A. J., Hendry, M. A.,
1487 Robertson, E., and Smout-Day, K.: JULES-GL7: the Global Land configuration of the Joint UK Land
1488 Environment Simulator version 7.0 and 7.2, *Geosci. Model Dev.*, 13, 483-505, 10.5194/gmd-13-483-2020,
1489 2020.

1490
1491 Wohlfahrt, G., Bahn, M., Haubner, E., Horak, I., Michaeler, W., Rottmar, K., Tappeiner, U., and Cernusca, A.:
1492 Inter-specific variation of the biochemical limitation to photosynthesis and related leaf traits of 30 species from
1493 mountain grassland ecosystems under different land use, *Plant, Cell & Environment*, 22, 1281-1296,
1494 10.1046/j.1365-3040.1999.00479.x, 1999.

1495
1496 Xiao, Z., Liang, S., Wang, J., Xiang, Y., Zhao, X., and Song, J.: Long-Time-Series Global Land Surface
1497 Satellite Leaf Area Index Product Derived From MODIS and AVHRR Surface Reflectance, *IEEE Transactions*
1498 *on Geoscience and Remote Sensing*, 54, 5301-5318, 10.1109/TGRS.2016.2560522, 2016.

1499
1500 Yamaguchi, D. P., Nakaji, T., Hiura, T., and Hikosaka, K.: Effects of seasonal change and experimental
1501 warming on the temperature dependence of photosynthesis in the canopy leaves of *Quercus serrata*, *Tree*
1502 *Physiology*, 36, 1283-1295, 10.1093/treephys/tpw021, 2016.

1503
1504 Yamori, W., Hikosaka, K., and Way, D. A.: Temperature response of photosynthesis in C3, C4, and CAM
1505 plants: temperature acclimation and temperature adaptation, *Photosynthesis Research*, 119, 101-117,
1506 10.1007/s11120-013-9874-6, 2014.

1507
1508 Yang, R., Friedl, M. A., and Ni, W.: Parameterization of shortwave radiation fluxes for nonuniform vegetation
1509 canopies in land surface models, *Journal of Geophysical Research: Atmospheres*, 106, 14275-14286, 2001.

1510
1511 Zeng, Z., Piao, S., Li, L. Z. X., Zhou, L., Ciais, P., Wang, T., Li, Y., Lian, X., Wood, E. F., Friedlingstein, P.,
1512 Mao, J., Estes, L. D., Myneni, Ranga B., Peng, S., Shi, X., Seneviratne, S. I., and Wang, Y.: Climate mitigation
1513 from vegetation biophysical feedbacks during the past three decades, *Nature Climate Change*, 7, 432-436,
1514 10.1038/nclimate3299, 2017.

1515
1516 Zhang, X. W., Wang, J. R., Ji, M. F., Milne, R. I., Wang, M. H., Liu, J.-Q., Shi, S., Yang, S.-L., and Zhao, C.-
1517 M.: Higher Thermal Acclimation Potential of Respiration but Not Photosynthesis in Two Alpine *Picea* Taxa in
1518 Contrast to Two Lowland Congeners, *PLOS ONE*, 10, e0123248, 10.1371/journal.pone.0123248, 2015.

1519
1520 Zhang, Y. and Schaap, M. G.: Weighted recalibration of the Rosetta pedotransfer model with improved
1521 estimates of hydraulic parameter distributions and summary statistics (Rosetta3), *Journal of Hydrology*, 547, 39-
1522 53, 10.1016/j.jhydrol.2017.01.004, 2017.

1523
1524 Zhao, M. and Running, S. W.: Drought-Induced Reduction in Global Terrestrial Net Primary Production from
1525 2000 Through 2009, *Science*, 329, 940-943, 10.1126/science.1192666, 2010.

1526

1527 Zhao, M., Running, S. W., and Nemani, R. R.: Sensitivity of Moderate Resolution Imaging Spectroradiometer
1528 (MODIS) terrestrial primary production to the accuracy of meteorological reanalyses, *Journal of Geophysical*
1529 *Research: Biogeosciences*, 111, 10.1029/2004JG000004, 2006.
1530
1531 Zhao, M., Heinsch, F. A., Nemani, R. R., and Running, S. W.: Improvements of the MODIS terrestrial gross and
1532 net primary production global data set, *Remote Sensing of Environment*, 95, 164-176,
1533 10.1016/j.rse.2004.12.011, 2005.
1534
1535 Ziehn, T., Kattge, J., Knorr, W., and Scholze, M.: Improving the predictability of global CO₂ assimilation rates
1536 under climate change, *Geophysical Research Letters*, 38, 10.1029/2011GL047182, 2011.
1537